Acta Pharmaceutica Sinica B 2025;15(3):1552−1570

Chinese Pharmaceutical Association
Institute of Materia Medica, Chinese Academy of Medical Sciences

Acta Pharmaceutica Sinica B

www.elsevier.com/locate/apsb
www.sciencedirect.com

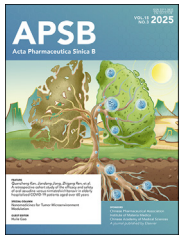

ORIGINAL ARTICLE

BRD4 regulates m^{6}A of ESPL1 mRNA *via* interaction with ALKBH5 to modulate breast cancer progression

Haisheng Zhang[a,†], Linlin Lu[b,†], Cheng Yi[a,†], Tao Jiang[a,c,†], Yunqing Lu[a], Xianyuan Yang[a], Ke Zhong[a], Jiawang Zhou[a], Jiexin Li[a], Guoyou Xie[a], Zhuojia Chen[d], Zongpei Jiang[e], Gholamreza Asadikaram[f], Yanxi Peng[g,*], Dan Zhou[h,*], Hongsheng Wang[a,*]

[a]*Guangdong Provincial Key Laboratory of Chiral Molecule and Drug Discovery; State Key Laboratory of Anti-Infective Drug Discovery and Development; School of Pharmaceutical Sciences, Sun Yat-sen University, Guangzhou 510006, China*
[b]*Institute of Medical Sciences, the Second Hospital, Cheeloo College of Medicine, Shandong University, Jinan 250033, China*
[c]*School of Life Sciences, Zhuhai College of Science and Technology, Zhuhai 519041, China*
[d]*Sun Yat-sen University Cancer Center; State Key Laboratory of Oncology in South China; Collaborative Innovation Center for Cancer Medicine, Guangzhou 510060, China*
[e]*Department of Nephrology, the Sixth Affiliated Hospital, Sun Yat-Sen University, Guangzhou 510655, China*
[f]*Endocrinology and Metabolism Research Center, Institute of Basic and Clinical Physiology Sciences, Kerman University of Medical Sciences, Medical University Campus, Kerman 7616914115, Iran*
[g]*School of Public Health, Xiangnan University, Chenzhou 423000, China*
[h]*Department of Breast Surgery, the First People's Hospital of Foshan, Foshan 528100, China*

Received 25 June 2024; received in revised form 18 September 2024; accepted 15 November 2024

KEY WORDS

BRD4;
ALKBH5;
ESPL1;

Abstract The interaction between m^{6}A-methylated RNA and chromatin modification remains largely unknown. We found that targeted inhibition of bromodomain-containing protein 4 (BRD4) by siRNA or its inhibitor (JQ1) significantly decreases mRNA m^{6}A levels and suppresses the malignancy of breast cancer (BC) cells *via* increased expression of demethylase AlkB homolog 5 (ALKBH5). Mechanistically,

*Corresponding authors.
E-mail addresses: whongsh@mail.sysu.edu.cn (Hongsheng Wang), zhoudanms@hotmail.com (Dan Zhou), yanxipeng@xnu.edu.cn (Yanxi Peng).
[†]These authors made equal contributions to this work.
Peer review under the responsibility of Chinese Pharmaceutical Association and Institute of Materia Medica, Chinese Academy of Medical Sciences.

https://doi.org/10.1016/j.apsb.2024.12.037

TRIM21;
RALY;
Cell cycle;
Breast cancer;
m^{6}A

inhibition of BRD4 increases the mRNA stability of ALKBH5 *via* enhanced binding between its 3′ untranslated regions (3′UTRs) with RNA-binding protein RALY. Further, BRD4 serves as a scaffold for ubiquitin enzymes tripartite motif containing-21 (TRIM21) and ALKBH5, resulting in the ubiquitination and degradation of ALKBH5 protein. JQ1-increased ALKBH5 then demethylates mRNA of extra spindle pole bodies like 1 (ESPL1) and reduces binding between *ESPL1* mRNA and m^{6}A reader insulin like growth factor 2 mRNA binding protein 3 (IGF2BP3), leading to decay of *ESPL1* mRNA. Animal and clinical studies confirm a critical role of BRD4/ALKBH5/ESPL1 pathway in BC progression. Further, our study sheds light on the crosstalks between histone modification and RNA methylation.

1. Introduction

Uncontrolled proliferation of cancer cells is linked to 'transcription addiction', which involves both chromatin regulators and the basal transcription machinery[1]. Histone modification has notable effects on gene expression[2]. Bromodomain-containing protein 4 (BRD4), a member of the bromodomain and extraterminal (BET) family, modulates gene transcription *via* recruitment of lineage-specific transcriptional regulators[3,4]. BRD4 can be recruited to distinct genomic loci *via* interaction between its tandem bromodomains and acetylated lysines on histones, including histone H4 acetylated at lysine residues 5, 8, 12 and/or 16[5], or transcription factors. It can also occupy distal enhancer RNA (eRNA) regions to regulate transcription[6]. Many small-molecule inhibitors, such as JQ1, I-BET and their derivatives, inhibit BRD4 to suppress cancer progression and some of them have entered clinical trials[7−11]. Although BRD4 generally serves as an RNA polymerase II (Pol II)-dependent transcriptional regulator, it also displays selective effects on gene expression *via* undefined mechanisms[12]. Further, little is known about factors that are directly required for BRD4 function.

N^6-Methyladenosine (m^{6}A) is the most widespread and highly conserved mRNA modification regulated mainly by writer, eraser, and reader proteins[13]. The mRNA m^{6}A modification is installed by methyltransferase-like 3 (METTL3)[14] and can be removed by demethylases Fat mass and obesity-associated protein (FTO) and AlkB homolog 5 (ALKBH5)[15−17]. It plays a critical role in RNA processing including RNA splicing, export, stability and translation[18]. Dysregulation of m^{6}A-methylated mRNA also regulates cancer development[19]. Recent studies indicate that m^{6}A is implicated in diverse biological processes of cancer cells glycolysis[20], and chemoresistance[21].

m^{6}A is also found on chromatin-associated RNA and the chromatin binding of methyltransferases may affect transcription[22−24]. Recent studies confirmed the roles of m^{6}A in the regulation of chromatin state and transcription[25−27]. For example, m^{6}A is co-transcriptionally added onto chromatin-associated regulatory RNAs (carRNAs) and the decrease of m^{6}A on carRNAs increases their abundance to enhance chromatin accessibility[25]. In addition, the repressive histone mark H3K9me2 is specifically removed by the induction of m^{6}A-modified transcripts, due to m^{6}A reader YTH domain containing 1 (YTHDC1) physically interacting with and recruiting lysine demethylase 3B (KDM3B) to promote H3K9me2 demethylation and gene expression[26]. However, the interaction between m^{6}A-methylated RNA and chromatin modification and related biological functions remain largely unknown.

Here we show that targeted inhibition of BRD4 *via* siRNA or small-molecule inhibitor JQ1 could suppress malignancy of breast cancer (BC) cells and mRNA m^{6}A *via* upregulation of ALKBH5. We demonstrated that inhibition of BRD4 increases mRNA and protein stability of ALKBH5. RNA-binding protein RALY and E3 ubiquitin ligase tripartite motif containing-21 (TRIM21) were, respectively, involved in BRD4-regulated ALKBH5 mRNA and protein stability. Further, extra spindle pole bodies like 1 (ESPL1) mediates BRD4/ALKBH5-regulated cell cycle and BC progression. Collectively, our studies reveal an important role of BRD4 in determining specific and dynamic deposition of m^{6}A in mRNA.

2. Materials and methods

2.1. Plasmid, siRNA and transfection

BRD4 plasmid was purchased from Addgene (90,331), and the histone deacetylase 2 (HDAC2) plasmid and empty vector were as a gift from Professor Jiemin Wong at the East China Normal University. The BRD4 deletion constructs were generated as reported previously[28]. The ESPL1 plasmid was constructed by inserting the cDNA of ESPL1 into the backbone plasmid pcDNA3.1 to generate pcDNA/ESPL1 for overexpression. The siRNAs for BRD2/3/4 were synthesized by the Guangzhou Ruibo Company. The siRNAs for TRIM21, RALY, TAR DNA binding protein (TARDBP), U2 small nuclear RNA auxiliary factor 2 (U2AF2), and insulin like growth factor 2 mRNA binding protein 3 (IGF2BP3) were synthesized by Shanghai Oobio Company. The sequences of siRNA were provided in the Supporting Information For plasmid transfection, cells were transfected with vector control or plasmid constructs using Lipofectamine 3000 (Cat# L3000001, Invitrogen, CA, USA). For siRNA transfection, siRNA negative control (si-NC) or specific siRNA was delivered to cells using Lipofectamine 3000 (Cat# L3000001, Invitrogen, CA, USA) with the working concentration of 50 nmol/L. The siRNA sequences are as follows: si-NC, 5′- UUC UCC GAA CGU GUC ACG U-3′; si-BRD2, 5′- CAC UUG GCC UGC AUG ACU A-3′; si-BRD3, 5′-GGA GAG CUC UUC GGA CUC A-3′; si-BRD4, 5′-GCU CAA GAC ACU AUG GAA A-3′; si-ALKBH5, 5′-GGA UAU GCU GCU GAU GAA A-3′; si-TRIM21-1, 5′- GUG AAC AAC CUU AAA GAA A-3′; si-TRIM21-2, 5′-GAG CAU ACC UGG AAA UGA A-3′; si-RALY, 5′- GCA AUG UAA CCA ACA AGA A-3′; si-TARDBP, 5′-CCG AAG AUG AGA ACG AUG-3′; si-U2AF2, 5′- CCA UGA UGG AUU UCU UCA A-3′; si-IGF2BP3-1, 5′- CCU UGA AAG UAG CCU AUA U-3′; si- IGF2BP3-2, 5′- GCA GGA AUU GAC GCU GUA U-3′.

2.2. Cell line and cell culture

Human MDA-MB-231, BT-549,A549 and HepG2 cancer cells were purchased from the American Type Culture Collection (ATCC, Manassas, VA, USA) and maintained in our lab by ATCC-recommended medium (Gibco) supplemented with 10% fetal bovine serum (FBS) under a humidified 5% CO_2 atmosphere incubator at 37 °C. The breast cancer lung metastasis cell line was established in our previous study *via* three rounds of *in vivo* selection of BC cells[29]. The lung metastasis BC cells were named as MDA-MB-231^{LMF2} or BT-549 ^{LMF3} cells, respectively. To generate stable cell lines with continuous suppression of ALKBH5 and METTL3, cells were transfected with lentivirus-shRNA for negative control, ALKBH5, and METTL3, respectively, before selection with puromycin.

2.3. LS−MS/MS for m^6A measurement

The method for m^6A measurement was conducted with our previous studies[20]. Briefly, mRNA was purified from the total RNA using oligo dT magnetic beads. About 200 ng of purified mRNAs were incubated with nuclease P1 (Cat# N8630, 0.5 U, Sigma) in 26 μL reaction system containing 20 mmol/L NH_4Ac (pH = 5.3) at 42 °C for 2 h, followed by the addition of NH_4HCO_3 (1 mol/L, 3 μL) and alkaline phosphatase (1 μL, 1 U/μL; Sigma) and incubation at 37 °C for 2 h. After neutralization with 1 μL HCl (3 mol/L), samples were diluted to 80 μL and filtered by 0.22 μm filter (Millipore). All samples (10 μL for each injection) were separated by a C18 column (Agilent) using reverse-phase ultra-performance liquid chromatography and analyzed by a Thermo Tsq Quantum Access Max using a positive electrospray ionization mode. All nucleosides were quantified by using retention time and ion mass transitions of 268.0 to 136.0 (A) and 282.1 to 150.0 (m^6A). Quantification was calculated using standard curves from standards running in the same batch. The ratio of m^6A to A was calculated based on calibration curves.

2.4. Dot blot for m^6A

mRNA was enriched using the GenElute messenger RNA (mRNA) Miniprep Kit (Cat# MRN10, Sigma−Aldrich) and the RiboMinus Transcriptome Isolation Kit (human/mouse; Cat# K155001, Thermo Fisher Scientific). After denaturing 5 min at 70 °C, equal amounts of serially diluted mRNA were added into an Amersham Hybond N+ membrane (Cat# RPN1520N, GE Healthcare) and cross-linked into auto-cross-linker three times under auto-cross-linking mode. The membrane was blocked with 5% milk in 1 × PBST for 1 h at room temperature and then inducted with anti-m^6A antibody (Cat# 202,003, SySy) overnight (4 °C). The membrane was washed according to the standard protocol. Horseradish peroxidase-conjugated anti-rabbit immunoglobulin G (Cat# 7074, Cell Signaling Technology) was diluted 1:5000 and incubated with the membranes for 1 h at room temperature. Membranes were developed with a 3,3′-diaminobenzidine peroxidase substrate kit (Cat# 36201ES03, Yeasen Biotechnology, Shanghai, China) to detect the signal.

2.5. Western blot analysis

After treatment, cells were washed three times with ice-cold phosphate buffer solution (PBS) and then lysed in lysis buffer containing 50 mmol/L Tris−HCl (pH 7.6), 150 mmol/L NaCl, 1 mmol/L EDTA, 1%NP-40, 0.5%Na-deoxycholate, 5 mg/mL aprotinin, 5 mg/mL leupeptin, and 1 mmol/L phenylmethylsulfonyl fluoride for 20 min. Lysates were cleared by centrifugation. Equal amounts of protein samples were loaded per well and separated on sodium dodecyl sulfate-polyacrylamide gel electrophoresis (SDS-PAGE), and then electrophoretically transferred onto polyvinylidene fluoride (PVDF) membranes. Following blocking with 5% non-fat milk at room temperature for 2 h, membranes were incubated with primary antibodies (1:1000 dilution) at 4 °C overnight and then incubated with horseradish peroxidase (HRP)-conjugated secondary antibodies (1:5000 dilution) for 2 h at room temperature. The primary antibodies used in this study were ALKBH5 (Millipore, ABE547), BRD4 (CST, 13440S), METTL3 (CST, 86132S), METTL14 (CST, 51,104), FTO (Abcam, ab126605), GAPDH (Bioworld, AP0063), c-Myc (Thermo Fisher, MA1-980), ubiquitin (Abcam, ab7254), TRIM21(Abclonal, A1957), vimentin (CST, 5741S), fibronectin (FN, Santa, sc-8422), HDAC2 (ABclonal, A2084), Flag (Sigma, 7425/1804), pan-Kac (CST, 9814), RALY (Abcam, ab170105), IGF2BP3 (Proteintech, 14642-1-AP), BRD2 (Proteintech, 22236-1-AP), BRD3 (Proteintech, 11859-1-AP), TARDBP (Santa Cruz, 41-7.1), U2AF2 (Proteintech, 68166-1-Ig), AURKA (Proteintech, 66757-1-Ig), E2F2 (Sigma, SAB1405736), and ESPL1 (Sigma, WH0009700M1). Specific immune complexes were detected using Western Bright ECL Reagent (Cat# K-12045-C20, Advansta). The quantitative analysis of Western blot analysis was performed according to the previous study[30]. Briefly, the intensity of the bands on the blots was measured using Image Lab (Bio-Rad). The intensity values of target proteins were divided by the intensity values of internal control (GAPDH or α-tubulin). The optical density value for each sample was then normalized to that of one of the control samples in the respective gel. The obtained intensity value from control cells was set to 100% with $n = 3$ for each group unless otherwise specified. One of representative Western blot experiments is shown.

2.6. Cell proliferation assay

Cell proliferation was evaluated using a CCK-8 cell viability assay system according to the manufacturer's protocol. Briefly, cells were seeded in 96-well plates at a density of 1×10^4 cells per well in 10% FBS-supplemented medium and then treated drugs. After treatment under indicated conditions, 10 μL of CCK-8 solution was added to each well. The plates were incubated for another 2 h, and the absorbance was measured at 450 nm using a microplate reader. The experiments were repeated six times.

2.7. In vitro wound healing assay and Transwell assay

For the wound-healing assay, cells were seeded in 6-well plates and grown to 80% confluency. Cells were scratched using a 10-μL pipette tip. After being washed three times with PBS to remove cell debris, cells were cultured in FBS-free medium to block cell growth, and then exposed to appropriate drugs. Recovery from the scratched wound was monitored using a microscope. Each migration experiment was carried out in duplicate and repeated in three independent experiments. The relative migration rate was calculated using Image J software. Distance migrated was calculated by subtracting the average distance between wound edges from that at the beginning.

Cell invasion assay was conducted using 24-well Transwell plates (8-μm pore size, Cat#3428, Corning). Briefly,

polycarbonate filters pre-coated with Matrigel Matrix (20 mg/mL, Cat# 356,234, BD Biosciences) were used for invasion assay. Cells (2×10^4) in 300 μL FBS free medium were seeded in the upper chamber. Then 500 μL medium with 10% FBS was added to the lower chamber and served as a chemotactic agent. After incubation for the indicated time period. The number of penetrated cells was counted under a phase contrast microscope (five random fields per chamber). Invasion assays were carried out with at least 5 individual experiments.

2.8. RNA extraction and quantitative real-time PCR

After treatment as indicated. Total mRNA from cells was extracted with TRIZOL reagent (Agbio, AG21102). First strand of cDNA was generated from 2 μg total RNA Evo M-MLV RT Premix (Cat# AG11706, AGbio). Quantitative real-Time PCR was run on C1000 Touch Thermal Cycler (Bio-Rad) using validated primers and SYBR Green Premix pro Taq HS (Cat# AG11701, AGbio) for detection. Primers for targeted genes were as follow:

GAPDH, forward 5′-GCACCGTCAAGGCTGAGAAC-3′ and reverse 5′-TGGTGAAGACGCCAGTGGA-3′.

ALKBH5, forward 5′-CGCTGCCGCCGAACCTTAC-3′ and reverse 5′-GGATGCCGCTCTTCACCTTGC-3′.

Pre-*ALKBH5*, forward 5′-GCCCAGAGGTGATGAGCAGTAAAG-3′ and reverse 5′-TGCCACCAACACCAACTGAAGTC-3′.

HDAC2, forward 5′-AAGTCTGCTACTACTACGACG-3′ and reverse 5′-TTATGGGTCATGCGGATTCTAT-3′.

TRIM21, forward 5′-TCCTTCTACAACATCACTGACC-3′ and reverse 5′-CAATATTCAGTGGACAGAGGGT-3′.

HPRT1, forward 5′-TCGAGATGTGATGAAGGAGATG-3′ and reverse 5′-CAGCAAAGAATTTATAGCCCCC-3′.

RALY, forward 5′-GCCTTTGTTCAGTACTCCAATG-3′ and reverse 5′-GAAGAGCCTGTATATGGCAGAT-3′.

TARDBP, forward 5′-AAAGAAGTGGAAGATTTGGTGC-3′ and reverse 5′-GGTTTTGGTTATTACCCGATGG-3′.

U2AF2, forward 5′-GAGTATGAGGAGATCGTGGAG-3′ and reverse 5′-GAACTCCACAAAGATCTTTCCG-3′.

ESPL1, forward 5′-CTCTGCTGCTGTCTGTGCTTCG-3′ and reverse 5′-GAGGTTGTTTGACGGGAGGCTAAG-3′.

BRD4, forward 5′-CTCCCCGCTTATGATACATTCC-3′ and reverse 5′-GTTTCTTAGGCTGGACGTTTTG-3′.

AURKA, forward 5′- GAGGTCCAAAACGTGTTCTCG-3′ and reverse 5′- ACAGGATGAGGTACACTGGTTG-3′.

E2F2, forward 5′- CGTCCCTGAGTTCCCAACC-3′ and reverse 5′- GCGAAGTGTCATACCGAGTCTT-3′.

Levels of precursor mRNA of *ALKBH5* were measured by qRT-PCR using primers spanning the exon 1 and intron 2. *GAPDH* was used as an endogenous control for normalization. Expression levels were calculated using the $2^{-\Delta\Delta Ct}$ method. Three independent experiments were performed.

2.9. Protein stability

To measure protein stability, cells were treated with cycloheximide (CHX, Item NO 14126, Cayman Chemical, USA) at final concentration 20 μg/mL for indicated times. The expression of protein was measured through Western blot analysis.

2.10. mRNA stability

To measure RNA stability in breast cancer cells, actinomycin D (Act-D, Catalog GC16866, Glpbio, USA) at 10 μg/mL was added to cells. After incubation at the indicated times, cells were collected, and RNA was isolated for real-time PCR. Half-life ($t_{1/2}$) of precursor or mature mRNA was calculated using ln2/slope and GAPDH was used for normalization.

2.11. Confocal

Cells were cultured on confocal dishes and then exposed to JQ1 for the indicated time period. Afterward, cells were then washed three times with 1 × PBS, fixed in 4% paraformaldehyde for 30 min, and permeabilized with 0.3% Triton X-100 for 15 min. After blocking with goat serum for 30 min, cells were incubated with primary antibody against ALKBH5, BRD4 or TRIM21 overnight. The dishes were washed three times with 1 × PBS and incubated with Alexa Fluor 488 or Alexa Fluor 594-conjugated secondary antibodies for 1 h at room temperature. Nuclei were stained with DAPI (10 mg/mL) for 10 min. Samples were examined with Confocal Laser Scanning Microscopy (Olympus, FV3000).

2.12. Immunoprecipitation

After lysis and centrifugation, 10% of the crude lysate was collected as input. Equal amounts of protein were immunoprecipitated with a preclearing and incubated overnight at 4 °C with the primary antibody. As a control, immunoprecipitation with IgG was also conducted. Protein A + G magnetic beads were added and incubated at 4 °C for 3 h. After 4 washes with lysis buffer and once with PBS plus inhibitors, pellets were resuspended in 1 × loading buffer, and boiled in a metal bath for 5 min. The expression of proteins was measured by Western blot analysis.

2.13. Luciferase reporter assay

To evaluate the effect of 3′UTR on ALKBH5 expression. The wild type 3′UTR of ALKBH5 or HPRT1 was inserted into the F-luc coding region. The pmirGLO-ALKBH5-3′UTR-WT, pmirGLO-HPRT1-3′UTR-WT and vector control constructs were transfected into cells for 24 h. Firefly luciferase (F-luc) and Renilla luciferase (R-luc) activities were assayed by Dual-Lumi II (Cat# RG089M, Beyotime) according to the manufacturers' instructions.

2.14. RIP-RT-PCR

The RIP-RT-PCR was conducted according to the previous studies[31–33]. For RNA immunoprecipitation, cells were irradiated twice with 400 mJ/cm^2 at 254 nm by Stratalinker on ice and lysed in high salt lysis buffer (300 mmol/L NaCl, 0.2% NP-40, 20 mmol/L Tris−HCl PH 7.6, 0.5 mmol/L DTT, protease inhibitor cocktail (1 tablet/50 mL), and RNase inhibitor (1:200) at 4 °C for 30 min. After treatment with, or without, 1 U RNase T1 for 15 min at 24 °C, 10% supernatant was collected as input. Remaining supernatant was incubated with anti-YTHDF1 antibody, anti-m^{6}A, anti-RALY, anti-IGF2BPs, or IgG-conjugated protein A/G Magnetic Beads in 500 mL 1 × IP buffer supplemented with RNase inhibitors at 4 °C overnight. Bound RNAs were immunoprecipitated with beads and treated with 100 μL of elution buffer (5 mmol/L Tris−HCl pH 7.5, 1 mmol/L EDTA pH 8.0, 0.05% SDS, 20 mg/mL Proteinase K) for 2 h at 50 °C, and RNA was recovered with phenol: chloroform extraction followed by ethanol precipitation. Proteinase K treatment was performed after reverse-cross linking and before RNA isolation and was

sufficient to remove all proteins. The reverse transcription by use of M-MLV reverse transcriptase can generate cDNA from the extracted RNA. RIP enrichment ratio of a transcript was calculated as ratio of its amount in IP to that in the input, derived from same amounts of cells.

2.15. Cell cycle analysis

To analyze cell cycle, cells were seeded in a 6-well plate 1 day before treatment. After treatment with appropriate drugs, cells were trypsinized and collected in a 1.5 mL tube, washed once with PBS. The cells were fixed in 75% ethyl alcohol overnight. The next day, the cells were washed once with PBS, stained with 20 μg/mL propidium iodide (PI, Cat#P4170, sigma) in PBS. Cell cycle was analysis analysed by flow cytometry. The data was analysed by Modfit. G0/G1 and G2/M phase gates were selected manually based on the cell count *vs.* propidium iodide intensity histogram.

2.16. Experimental animals and xenograft models

All animal experiments were conducted according to the guidelines of Institutional Animal Care and Use Committee, Sun Yat-sen University. Breast cancer cell model with high lung metastasis potential was established in our previous study (Approval No: SYSU-IACUC-2019-B237)[34]. The patient derived xenograft (PDX) model was also developed in our earlier research (Approval No.: SYSU-IACUC-2018-000127)[29]. The First Affiliated Hospital of Sun Yat-sen University approved the use of the patient sample (48 years old) diagnosed with stage IV (metastatic) triple-negative breast cancer (TNBC). Written consent was obtained from the patient prior to the use of the sample.

For xenograft model, the experiment has been approved by Affidavit of Approval of Animal Use Protocol, IACUC, SYSU (Approval No: SYSU-IACUC-2021-000155). Female BALB/c nude mice (4-week-old) were purchased from Gempharmatech (Jiangsu, China) Animal Center and raised under pathogen-free conditions. All animal experiments complied with the Sun Yat-sen University of Medicine Policy on Care and Use of Laboratory Animals. For the subcutaneous xenograft model, sh-control and sh-ALKBH5 MDA-MB-231 cells (5×10^6 per mouse, $n = 10$ for each group) were diluted in 100 μL of PBS and subcutaneously injected into immunodeficient female mice to investigate tumor growth. When the tumor was visible, the mice in each group were randomized into two additional groups of five mice with similar average xenograft tumor volumes and assigned to receive treatment with JQ1 [50 mg/kg in 10% (2-hydroxypropyl)-β-cyclodextrin, b.i.d.] or vehicle only ($n = 5$ xenografts per arm) by tail vein injection every day for 20 days. When tumor volume in the control group reached approximately 1000 mm^3, mice were euthanized, and tumors were removed and weighed for use in histology and further studies. The tumor volume was calculated as Eq. (1):

$$V = 1/2 \times \text{Larger diameter} \times \text{Smaller diameter} \quad (1)$$

Xenograft models were established in our previous study.

2.17. Immunohistochemistry (IHC)

Tumor tissues were fixed in formalin and embedded in paraffin. For immunohistochemical staining, sections were deparaffinized and hydrated. Endogenous peroxidase activity was blocked with 3% H_2O_2 in water for 20 min. Antigen retrieval was performed with 10 mmol/L citrate buffer (pH 6.0) for 30 min. Slides were incubated with goat serum (BOSTER) for 60 min to block nonspecific binding. Then, slides were incubated with primary antibodies overnight at 4 °C, washed in PBS twice and then incubated with goat anti-rabbit HRP-conjugated secondary antibodies for 2 h at room temperature. Finally, slides were incubated with 3,3′-diaminobenzidine and counterstained with hematoxylin. The protein expression was assessed semi-quantitatively by two independent authors. The intensity was scored on a scale of 0−3 as negative (0), weak (1), medium (2) or strong (3). The extent of the staining, defined as the percentage of positive stained areas of tumor cells relative to the whole tumor area, was scored on a scale of 0 (0%), 1 (1%−25%), 2 (26%−50%), 3 (51%−75%) and 4 (76%−100%). An overall protein expression score (overall score range, 0 to 12) was calculated by multiplying the intensity and positivity scores[21].

2.18. Sub-cellular fraction

Cytosolic and nuclear fractions of cells were separated by using a Subcellular Fractionation kit (P0028, Beyotime) according to the manufacturer's protocol. The levels of protein expression were measured by Western blot analysis.

2.19. Soft agar colony formation assay

Cancer cells were plated in the 6-well culture plate at a density of 1×10^3 cells/well and grown for 2 weeks in the incubator. 4% paraformaldehyde (Biosharp, BL539A) was added to fix the observed colonies at room temperature for 13−15 min. PFA was washed out with water. Colonies were stained with 1% crystal violet (Leagene, DZ0053) for 5 min for staining followed by imaging. The number of colonies was quantified by Image J software.

2.20. 4sU-labelling and RNA purification for nascent RNA measurement

Cells were cultured in the presence of 200 μmol/L 4-thiouridine (4sU, Cat# T4509, Sigma) for 2 h, lysed, and total RNA was extracted as described. 4sU-labeled RNA was biotinylated using EZ-Link Biotin-HPDP (Cat#21341, Pierce), dissolved in dimethylformamide (DMF) at a concentration of 1 mg/mL. For RNA precipitation and removal of unincorporated biotin-HPDP, a 1/10 volume 5 mol/L NaCl and an equal volume of absolute isopropanol were added to the aqueous phase and centrifuged for 20 min at 16,000 rpm (H1-16K, Hunan Kecheng Instrument and Equipment Co., Ltd., Changsha, China). RNA was resuspended in 100 μL RNase-free H_2O. Biotinylated RNA was captured using Dynabeads MyOne Streptavidin T1 beads (Cat#65601, Invitrogen, USA). Biotinylated RNA was incubated with 100 μL Dynabeads with rotation for 15 min at 25 °C. Beads were magnetically fixed and washed with 1 × Dynabeads washing buffer. RNA-4sU was eluted with 100 μL of freshly prepared 100 mmol/L dithiothreitol (DTT). RNA was recovered using the RNeasy Mini Kit (Cat#74104, Qiagen, Germany) and then subjected to RT-qPCR for analysis of nascent RNA.

2.21. RNA-seq and m^6A sequencing (m^6A-seq)

Total RNA was isolated from cells treated with or without JQ1 and purified by using RNeasy mini kit (Cat#74104, Qiagen, Germany). The construction of cDNA library with Tru-seq mRNA sample preparation kit (Cat# 20020594, Illumina, USA) was sequenced in Illumina platform. Cutadapt (v2.5) was used to trim adapters and filter for sequences, remaining reads were then aligned to the human Ensemble genome GRCh38 (mouse Ensemble genome GRCm38) using Hisat2 aligner (v2.1.0) under parameters: "–rna-strandness RF". The reads mapped the genome were calculated using featureCounts (v1.6.3). Differential gene expression analysis was performed using the DESeq2 R-package.

For m^6A-seq, the RNA was treated by chemical reagent (AM8740, ThermoFisher Scientific) to fragmentation. The fragmental RNA was incubated with m^6A antibody for immunoprecipitation according to the manufacture's instruction (Cat# 17-10499, MeRIP m^6A Kit, Merck Millipore, USA). m^6A-enriched RNA was used to generate the cDNA library in parallel with the input RNA, and then sequenced using the HiSeq 2000 system (Illumina, USA). All sequencing reads were mapped to a reference human genome sequence (NCBI 36.1 [hg19] assembly by TopHat (Version 2.0.6). m^6A peaks were identified using exomePeak R package (v2.13.2) under parameters: "PEAK_CUTOFF_PVALUE = 0.05, PEAK_CUTOFF_FDR = NA, FRAGMENT_LENGTH = 200". Differential m^6A peak were identified using exomePeak R package under parameters: "PEAK_CUTOFF_PVALUE = 0.05, PEAK_CUTOFF_FDR = NA, FRAGMENT_LENGTH = 200". GO and KEGG analysis were performed using cluster profile R package (v3.6.0). m^6A-RNA-related genomic features were visualized using Guitar R package (v1.16.0). Identified m^6A peaks which P value < 0.05 were chosen for the *de novo* motif analysis using homer (v4.10.4) under parameters: "-len 6 -rna". The variation of m^6A in specific transcript was analyzed according to method in the previous study[35]. The accession number for the high-throughput of RNA-seq and m^6A-seq data reported in this paper is GEO: GSE190541 (https://www.ncbi.nlm.nih.gov/geo/query/acc.cgi?acc=GSE190541).

2.22. Database (DB) search

We used Kaplan−Meier database (http://kmplot.com/analysis/) to assess overall survival (OS) and recurrence free survival (RFS) of BRD4/ALKBH5/ESPL1 axis. Difference between survival curves were determined by log-rank test that its P value < 0.05 were considered as statistically significant. Correlations between ALKBH5 expression in BC tissues and clinicopathological features were extracted from TCGA database and Oncomine database (www.oncomine.org). The data were analyzed with Pearson Chi-square (χ^2) test then.

2.23. Statistical analyses

All values were reported as mean ± standard deviation (SD) of at least three independent experiments unless otherwise specified. Data were analyzed by two tailed unpaired Student's t-test between two groups and by one-way ANOVA followed by Bonferroni test for multiple comparisons involved. Data distribution was assumed to be normal but this was not formally tested. The statistical analyses were performed using GraphPad. P-value of <0.05 was considered statistically significant.

Other detailed materials and methods are provided in the Supporting Information

3. Results

3.1. ALKBH5 is involved in BRD4-regulated m^6A and malignancy of BC cells

Our previous studies indicated that BRD4 was upregulated in BC cells and triggered the migration and invasion of cancer cells[29]. In the present study, we confirmed that JQ1, an inhibitor of BRD4, suppressed the colonization of both MDA-MB-231 and BT-549 cells (Fig. 1A). This might be due to JQ1-induced G2/M cell cycle arrest of BC cells (Supporting Information Fig. S1A). In addition, we found that JQ1 treatment increased doxorubicin (Dox) and cisplatin (CDDP) sensitivity of both MDA-MB-231 (Fig. 1B) and BT-549 (Fig. S1B) cells. These data confirmed that BRD4 regulates the malignancy of BC cells.

Recent studies confirmed the roles of m^6A in regulation of chromatin state and transcription[25−27]. However, it is unclear whether m^6A methylation is regulated by chromatin modified proteins. We further investigated the variation of m^6A levels in mRNAs of cancer cells treated with or without JQ1. Using liquid chromatography-linked tandem mass spectrometry (LC−MS/MS), we found that m^6A levels of mRNAs isolated from JQ1-treated MDA-MB-231 and BT-549 cells for 24 h were statistically ($P < 0.05$, t-test) less abundant than those from their corresponding control cells (Fig. 1C). The m^6A/A levels of mRNAs from MDA-MB-231 and BT-549 cells treated with JQ1 for 24 h decreased 30.1% and 26.9%, respectively. Similarly, LC−MS/MS showed that m^6A levels of mRNAs isolated from other BC cell such as MCF7 and SkBr3 and other cancer cells such as HepG2 and A549 cells treated with JQ1 were also statistically ($P < 0.05$, t-test) less abundant than those from their corresponding control cells (Fig. S1C). Moreover, JQ1 treatment decreased mRNA m^6A levels in a time-dependent manner in both MDA-MB-231 and BT-549 cells (Fig. 1C). Since JQ1 inhibits BRD2/3/4[36], we further knocked down individual expression of BRD2/3/4 in MDA-MB-231 cells (Fig. S1D). LC−MS/MS analysis showed that only si-BRD4, but not si-BRD2 or si-BRD3, suppressed mRNA m^6A levels in MDA-MB-231 cells (Fig. 1D). Further, overexpression of BRD4 in both MDA-MB-231 and BT-549 cells (Fig. S1E) increased m^6A levels of mRNAs (Fig. 1E). Consistently, the dot-blot assay confirmed that JQ1 treatment or si-BRD4, but not si-BRD2 or si-BRD3, suppressed mRNA m^6A levels in MDA-MB-231 cells (Fig. 1F). Collectively, these data show that BRD4 positively regulates mRNA m^6A in cancer cells including those from breast cancer.

Levels of mRNA m^6A modification are installed by METTL3/METTL14[14] and removed by demethylases FTO and ALKBH5[15,16]. We further analyzed the effects of JQ1 on these mRNA m^6A regulators. Western blot analysis showed that JQ1 treatment increased the expression of ALKBH5, but had no obvious effect on FTO, METTL3 or METTL14, in both MDA-MB-231 and BT-549 cells (Fig. 1G). Consistently, si-BRD4 increased (Fig. 1H), while overexpression of BRD4 decreased (Fig. S1F), the protein levels of ALKBH5 in both MDA-MB-231 and BT-549 cells. Further, JQ1 increased the expression of ALKBH5 in a time- and dose-dependent manner in both MDA-MB-231 (Fig. 1I) and BT-549 (Fig. S1G) cells. In addition, JQ1 also increased the levels of ALKBH5 in other BC cell such as

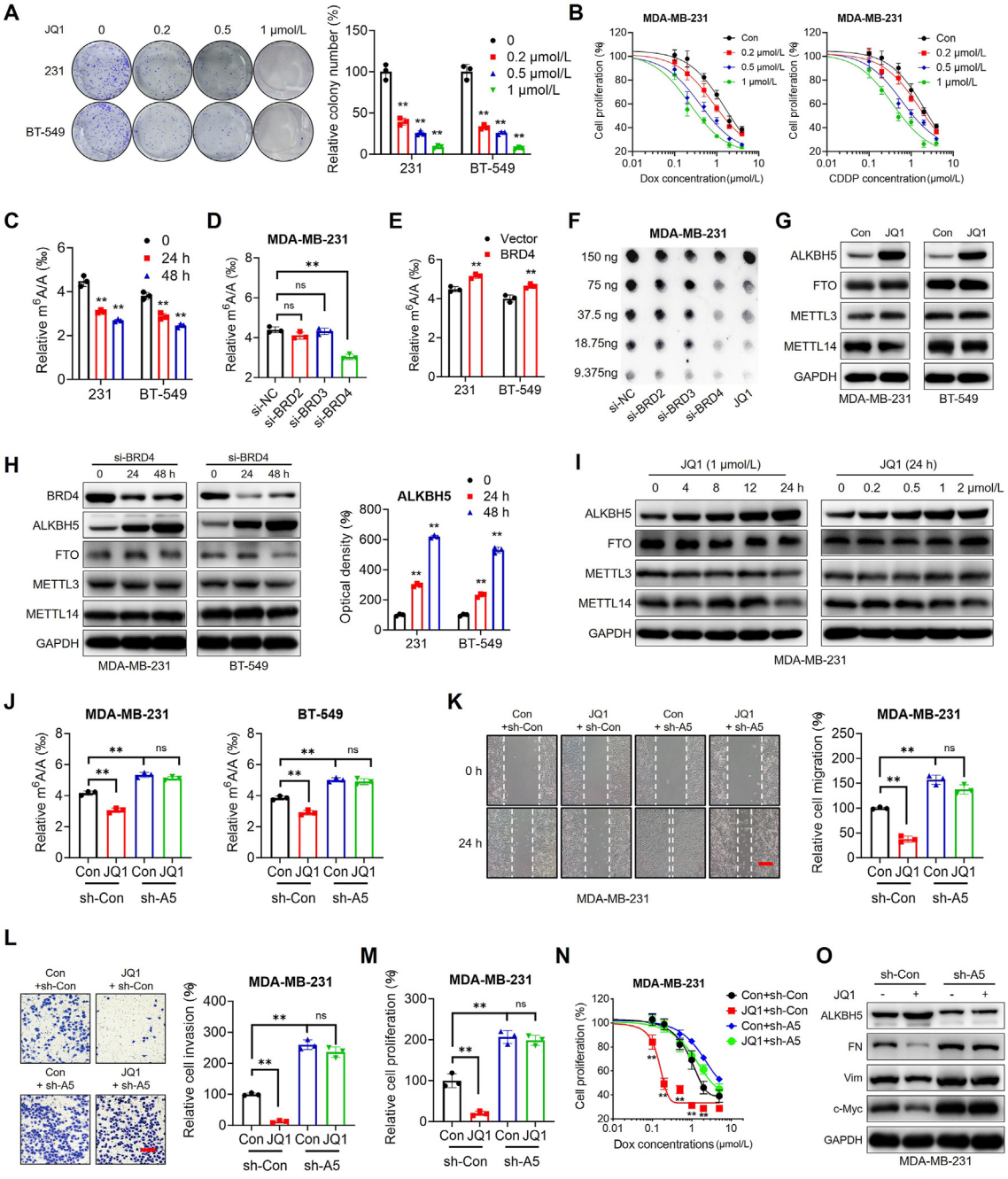

Figure 1 ALKBH5 is involved in BRD4-regulated m^{6}A and malignancy of BC cells. (A) The colonization capability of MDA-MB-231 and BT-549 cells treated with increasing concentrations of JQ1 were checked; (B) MDA-MB-231 cells were pre-treated with or without 0.2, 0.5, and 1 μmol/L JQ1 for 12 h, and further treated with increase concentration of Dox or CDDP for 48 h; (C) The m^{6}A/A ratio of mRNA in MDA-MB-231 and BT-549 cells treated with 1 μmol/L JQ1 for 24 or 48 h was checked by LC−MS/MS; (D) The m^{6}A/A ratio of mRNA in MDA-MB-231 cells transfected with si-NC or si-BRD2/3/4 for 24 h was checked by LC−MS/MS; (E) The m^{6}A/A ratio of mRNA in cells transfected with vector control or BRD4 constructs for 24 h was checked by LC−MS/MS; (F) The m^{6}A/A ratio of mRNA in MDA-MB-231 cells transfected with si-NC or si-BRD2/3/4 or treated with 1 μmol/L JQ1for 24 h was checked by dot-blot assay; (G) Protein expression in cells treated with or without 1 μmol/L JQ1 for 24 h was analyzed by Western blot analysis; (H) The protein expression in cells transfected with si-BRD4 for 24 or 48 h was checked by Western blot analysis (left) and quantitatively analyzed (right); (I) The protein expression in MDA-MB-231 cells treated with 1 μmol/L JQ1 for 0−24 h or increasing concentrations of JQ1 for 24 h was checked; (J) sh-Control or sh-ALKBH5 MDA-MB-231 and BT-549 cells were treated with or without 1 μmol/L JQ1 for 24 h. The m^{6}A/A ratio of mRNA was checked by LC−MS/MS; (K) sh-Control or sh-ALKBH5 MDA-MB-231 cells were treated with or without 1 μmol/L JQ1 for 24 h. The migration was checked by wound-healing assay (left) and quantitatively analyzed (right), scale bar: 200 μm; (L) sh-Control or sh-ALKBH5 MDA-MB-231 cells were treated with or without 1 μmol/L JQ1 for 24 h. The invasion was checked by Transwell assay (left) and quantitatively analyzed (right), scale bar: 200 μm; (M) Cell proliferation was checked in sh-Control or sh-ALKBH5 MDA-MB-231 cells treated with or without 1 μmol/L JQ1 for 24 h; (N) Cell proliferation of sh-Control

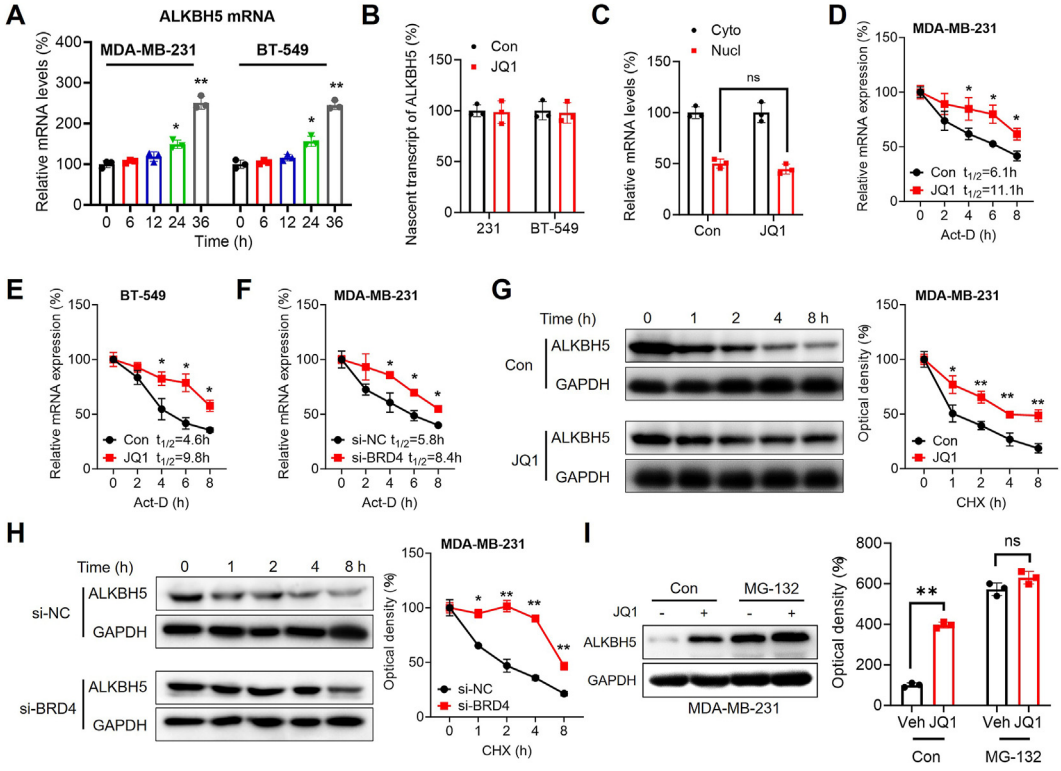

Figure 2 BRD4 regulates the mRNA and protein stability of ALKBH5. (A) The mature mRNA of ALKBH5 in cells treated with 1 μmol/L JQ1 for 0−36 h; (B) Nascent transcripts of ALKBH5 in cells treated with or without 1 μmol/L JQ1 for 24 h were analyzed by 4sU incorporation in the newly synthesized transcripts; (C) The relative levels of cytoplasmic versus nuclear *ALKBH5* mRNA in MDA-MB-231 cells treated with or without 1 μmol/L JQ1 for 24 h; (D, E) MDA-MB-231 (D) or BT-549 (E) cells were pre-treated with or without 1 μmol/L JQ1 for 24 h and further treated with Act-D for 0−8 h. The mRNA of *ALKBH5* was checked by qRT-PCR; (F) MDA-MB-231 cells were pre-transfected with si-NC or si-BRD4 for 24 h and further treated with Act-D for 0−8 h. The mRNA of *ALKBH5* was checked by qRT-PCR; (G) The protein of ALKBH5 in MDA-MB-231 cells pre-treated with or without 1 μmol/L JQ1 for 6 h and further treated with CHX for 0−8 h was checked by Western blot analysis (left) and quantitatively analyzed (right); (H) The protein of ALKBH5 in MDA-MB-231 cells pre-transfected with si-NC or si-BRD4 for 24 h and further treated with CHX for 0−8 h; (I) The protein of ALKBH5 in MDA-MB-231 cells pre-treated with or without MG-132 for 90 min and further treated with or without 1 μmol/L JQ1 for 24 h; Data are presented as mean ± SD from three independent experiments. $^{*}P < 0.05$, $^{**}P < 0.01$, ns, no significant, by Student's *t* test (two-side) as compared with the control group.

MCF7 and SkBr3 and other cancer cells such as HepG2 and A549 cells (Fig. S1H). As expected, si-BRD2 or si-BRD3 had no similar effects on the expression of ALKBH5 in either MDA-MB-231 or BT-549 cells (Fig. S1I).

We then investigated the potential roles of ALKBH5 in BRD4-regulated m^{6}A in BC cells. Our data showed that knockdown of ALKBH5 increased m^{6}A levels and attenuated JQ1-suppressed mRNA m^{6}A in MDA-MB-231 and BT-549 cells (Fig. 1J). Further, knockdown of ALKBH5 abolished JQ1-suppressed migration of MDA-MB-231 (Fig. 1K) and BT-549 (Fig. S1J) cells. Knockdown of ALKBH5 attenuated JQ1-suppressed invasion (Fig. 1L) and cell proliferation (Fig. 1M) and further increased Dox sensitivity (Fig. 1N) of MDA-MB-231 cells. It was further confirmed that knockdown of ALKBH5 attenuated JQ1-suppressed expression of mesenchymal markers vimentin and fibronectin as well as Myc oncogene in both MDA-MB-231 (Fig. 1O) and BT-549 (Fig. S1K) cells. To further confirm the essential roles of ALKBH5, MDA-MB-231 cells were transfected with ALKBH5 plasmid or a catalytically dead ALKBH5 H204A mutant (Fig. S1L). Our data showed that overexpression of ALKBH5 suppressed the migration and invasion while increasing the Dox sensitivity of MDA-MB-231 cells. While these effects were attenuated as for the catalytically dead ALKBH5 H204A mutant (Fig. S1M−S1O). Altogether, these data suggest that ALKBH5 is involved in BRD4-regulated m^{6}A and malignancy of BC cells.

3.2. *BRD4 regulates the mRNA and protein stability of ALKBH5*

We next investigated the mechanisms underlying BRD4-regulated expression of ALKBH5 in BC cells. qRT-PCR showed that JQ1 treatment increased mRNA expression of ALKBH5 in MDA-MB-231 and BT-549 cells after 12 h (Fig. 2A). However, JQ1 had no effect on ALKBH5 precursor mRNA levels in both MDA-MB-231 and BT-549 cells (Supporting Information Fig. S2A). Further,

or sh-ALKBH5 MDA-MB-231 cells pre-treated with or without 1 μmol/L JQ1 for 12 h and then further treated with an increasing concentration of Dox for 48 h; (O) The protein expression in sh-Control or sh-ALKBH5 MDA-MB-231 cells treated with or without 1 μmol/L JQ1 for 24 h. Data are presented as mean ± SD from three independent experiments. $^{**}P < 0.01$, ns, no significant, by Student's *t* test (two-side) as compared with the control group.

4-thiouridine (4sU) labeling of nascent transcripts showed no significant variations for the transcription of ALKBH5 in BC cells untreated or treated with JQ1 for 24 h (Fig. 2B). By separating nuclear and cytoplasmic RNAs, we found that JQ1 also had no effect on the nuclear export of ALKBH5 mRNA in MDA-MB-231 cells (Fig. 2C). We further examined the mRNA stability of ALKBH5 by treating cells with actinomycin D (Act-D), which binds the largest subunit of Pol II to block transcription[37]. The results showed that JQ1 treatment significantly increased the mRNA stability of ALKBH5 in both MDA-MB-231 (Fig. 2D) and BT-549 (Fig. 2E) cells. Consistently, si-BRD4 significantly increased the mRNA stability of ALKBH5 in MDA-MB-231 cells (Fig. 2F).

We further investigated potential effects of BRD4 on translation and post-translation of ALKBH5 in BC cells. Western blot analysis (Fig. S2B) showed that JQ1 increased nuclear localization of ALKBH5 without altering the relative ratio of cytoplasmic to nuclear levels of ALKBH5, which is due to the fact that JQ1 increased the total expression of ALKBH5. Our data showed that JQ1 increased the expression of ALKBH5 protein after 4 h (Fig. 1I and Fig. S1G), earlier than that of mRNA changes (Fig. 2A). We further checked the effect of JQ1 on protein stability of ALKBH5. The results showed that JQ1 treatment significantly increased the protein stability of ALKBH5 in both MDA-MB-231 (Fig. 2G) and BT-549 (Fig. S2C) cells. Similarly, si-BRD4 increased the protein stability of ALKBH5 in MDA-MB-231 cells (Fig. 2H). Treatment with MG132, a potent cell-permeable proteasome and calpain inhibitor, abolished JQ1-induced upregulation of ALKBH5 (Fig. 2I and Fig. S2D). These results suggest that BRD4 regulates both mRNA and protein stability of ALKBH5 in BC cells.

3.3. TRIM21 is essential for BRD4-regulated protein stability of ALKBH5

Our results showed that JQ1 could suppress ubiquitination and proteasome-mediated degradation of ALKBH5. To identify the ubiquitin ligases specifically targeting ALKBH5, MDA-MB-231 cells were transiently transfected with a plasmid encoding ALKBH5 or BRD4 along with the empty vector, followed by affinity purification using anti-ALKBH5 or anti-BRD4. Bound proteins were analyzed by LC−MS/MS[38]. We noticed that BRD4 could interact with ALKBH5 (Supporting Information Table S1). Among the 125 BRD4-bound proteins and 260 ALKBH5-bound proteins, 41 proteins were found to associate with both BRD4 and ALKBH5 (Fig. 3A). Among the 137 proteins involved in ubiquitin-mediated proteolysis (Table S1 and Supporting Information Table S2), we found TRIM21 was the only protein also identified among 125 BRD4-bound proteins and 260 ALKBH5-bound proteins (Fig. 3A). UBE2NL (ubiquitin conjugating enzyme E2 N like), a member of the ubiquitin-conjugating enzyme family, also associates with ALKBH5 (Fig. 3A).

IP with an anti-ALKBH5 antibody validated that endogenous ALKBH5, BRD4 and TRIM21 associate with one another in MDA-MB-231 cells (Fig. 3B). Consistently, ALKBH5, BRD4 and TRIM21 also bound to each other in BT-549 cells (Fig. S2E). JQ1 treatment decreased the binding between ALKBH5 and BRD4, and between ALKBH5 and TRIM21, in MDA-MB-231 cells (Fig. 3C). Similar results were obtained in BT-549 cells (Fig. S2F). Knockdown of BRD4 decreased the binding between ALKBH5 and TRIM21 (Fig. 3D), while knockdown of ALKBH5 had no effect on the binding between BRD4 and TRIM21, in MDA-MB-231 cells (Fig. 3E). Collectively, these data suggest that TRIM21/BRD4/ALKBH5 form a complex and BRD4 may serve as a scaffold for the binding between TRIM21 and ALKBH5 as previously proposed[39], similar to BRD9 interacting with RAD51 and RAD54[40].

Our data showed that JQ1 treatment decreased the expression of TRIM21 in both MDA-MB-231 and BT-549 cells (Fig. 3F). To confirm the roles of TRIM21 in BRD4-regulated protein stability of ALKBH5, we knocked down the expression of TRIM21 in BC cells (Fig. S2G). Our data showed si-TRIM21 significantly increased the protein expression of ALKBH5 in both MDA-MB-231 and BT-549 cells (Fig. 3G), with no effect on the mRNA expression (Fig. S2H). Consistently, LC−MS/MS analysis showed that si-TRIM21 significantly decreased m^6A levels of mRNAs in both MDA-MB-231 and BT-549 cells Fig. S2I). Further, si-TRIM21 significantly decreased ALKBH5 ubiquitination in both MDA-MB-231 (Fig. 3H) and BT-549 (Fig. 3I) cells. In addition, knockdown of TRIM21 increased the expression of ALKBH5 in a similar and non-additive manner to JQ1 treatment in both MDA-MB-231 (Fig. 3J) and BT-549 (Fig. S2J) cells, suggesting that they act in the same pathway.

Next, we investigated which domain of BRD4 is important for its interaction with ALKBH5 and TRIM21. To do so, we designed several BRD4 truncations (Fig. 3K)[28]. As shown in Fig. 3L, the C terminus of BRD4 was important for its interaction with TRIM21, whereas the BRD4 N terminus (bromodomains) was required for the interaction between BRD4 and ALKBH5 (Fig. 3L). Bromodomains are protein domains that recognize acetylated lysine residues[41]. We screened for acetyltransferases and deacetylases potentially involved in ALKBH5 interaction and found that HDAC2 was among ALKBH5-interacting proteins identified by LC−MS/MS (Fig. S2K). Overexpression of HDAC2 increased the protein expression of ALKBH5 (Fig. 3M) but decreased the acetylation of ALKBH5 (Fig. 3N). Further, overexpression of HDAC2 also decreased m^6A levels of mRNAs in both MDA-MB-231 and BT-549 cells (Fig. S2L). It seems that overexpression of HDAC2 decreased the interaction between ALKBH5 and BRD4, and between ALKBH5 and TRIM21 (Fig. 3O). Altogether, these results suggest that ALKBH5 is deacetylated in BC cells by HDAC2, and BRD4 can bind to acetylated ALKBH5 to recruit TRIM21, resulting in varied ALKBH5 ubiquitination and protein stability.

3.4. RALY is essential for BRD4-regulated mRNA stability of ALKBH5

Our data showed that JQ1 increased the mRNA stability of ALKBH5, which is primarily regulated by 3′ untranslated regions (3′UTRs) interacting with specific RNA-binding proteins (RBPs)[42]. To test whether the 3′UTR is involved in BRD4-regulated mRNA stability of ALKBH5, we generated a luminescence reporter by cloning the 3′UTR sequence of ALKBH5 mRNA to the 3′ end of the F-luciferase (F-Luc) gene in the pmiR-GLO plasmid (Fig. 4A). In cells treated with JQ1, we observed upregulation of more than 80% of the ALKBH5 3′UTR reporter activity relative to the control treatment. Similar upregulation of ALKBH5 3′UTR reporter activity was observed in cells transfected with si-BRD4 (Fig. 4A). This suggested that 3′UTR of ALKBH5 is involved in BRD4-regulated mRNA stability.

In order to identify RBPs that mediate BRD4-regulated mRNA stability, the RBPmap bioinformatics program was used to predict the presence of RBPs in ALKBH5 3′UTR with high stringency[43]. Among all of the potentially bound RBPs, we analyzed the top 15

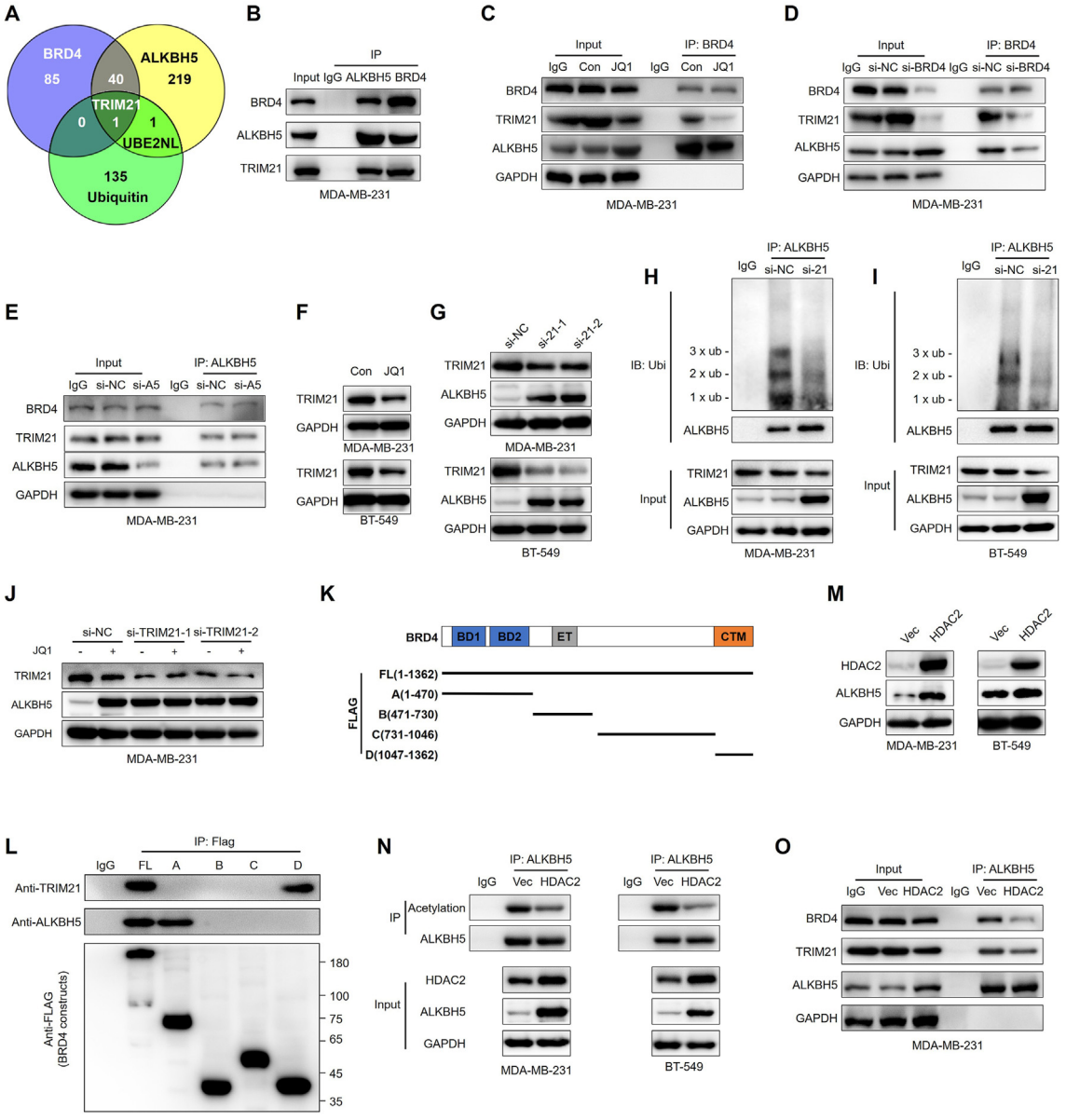

Figure 3 TRIM21 is essential for BRD4-regulated protein stability of ALKBH5. (A) Venn diagram shows substantial and significant overlaps among proteins involved in ubiquitin-mediated proteolysis and proteins bound with ALKBH5 and BRD4 in MDA-MB-231 cells; (B) Protein lysates of MDA-MB-231 cells were immunoprecipitated with BRD4 or ALKBH5 antibodies. The binding with other proteins was checked by immunoprecipitation; (C) MDA-MB-231 cells were treated with 1 μmol/L JQ1 for 24 h. Binding between ALKBH5 and TRIM21 or BRD4 was checked by immunoprecipitation; (D) MDA-MB-231 cells were transfected with si-NC or si-BRD4 for 24 h. Binding between ALKBH5 and TRIM21 or BRD4 was checked by immunoprecipitation; (E) MDA-MB-231 cells were transfected with si-NC or si-ALKBH5 for 24 h. Binding between BRD4 and TRIM21 or ALKBH5 was checked by immunoprecipitation; (F) The protein expression of TRIM21 in cells treated with or without 1 μmol/L JQ1 for 24 h; (G) The protein expression of ALKBH5 in cells transfected with si-NC or si-TRIM21 for 24 h; (H, I) The ubiquitination of ALKBH5 in MDA-MB-231 (H) or BT-549 (I) cells transfected with si-NC or si-TRIM21 for 24 h. An equal amount of ALKBH5 was loaded after IP according to a pre-Western blot; (J) The expression of ALKBH5 in MDA-MB-231 cells pre-transfected with si-NC or si-TRIM21 for 12 h and then further treated with or without 1 μmol/L JQ1 for 24 h; (K) Schematic diagram depicting a set of FLAG-tagged BRD4 expression constructs; (L) 293T cells were transfected with the indicated constructs of FLAG-BRD4, immunoprecipitation with anti-FLAG beads was performed. Blots were probed with the indicated antibodies of ALKBH5 or TRIM21; (M) The expression of ALKBH5 and HDAC2 in cells transfected with vector control or pT-HDAC2 for 24 h; (N) Acetylation of ALKBH5 in cells transfected with vector control or pT-HDAC2 for 24 h was checked by immunoprecipitation; (O) MDA-MB-231 cells were transfected with vector control or pT-HDAC2 for 24 h. The binding between ALKBH5 and BRD4 or between ALKBH5 and TRIM21 was checked by immunoprecipitation; Data are presented as mean ± SD from three independent experiments. $^{**}P < 0.01$, ns, no significant, by Student's t test (two-side).

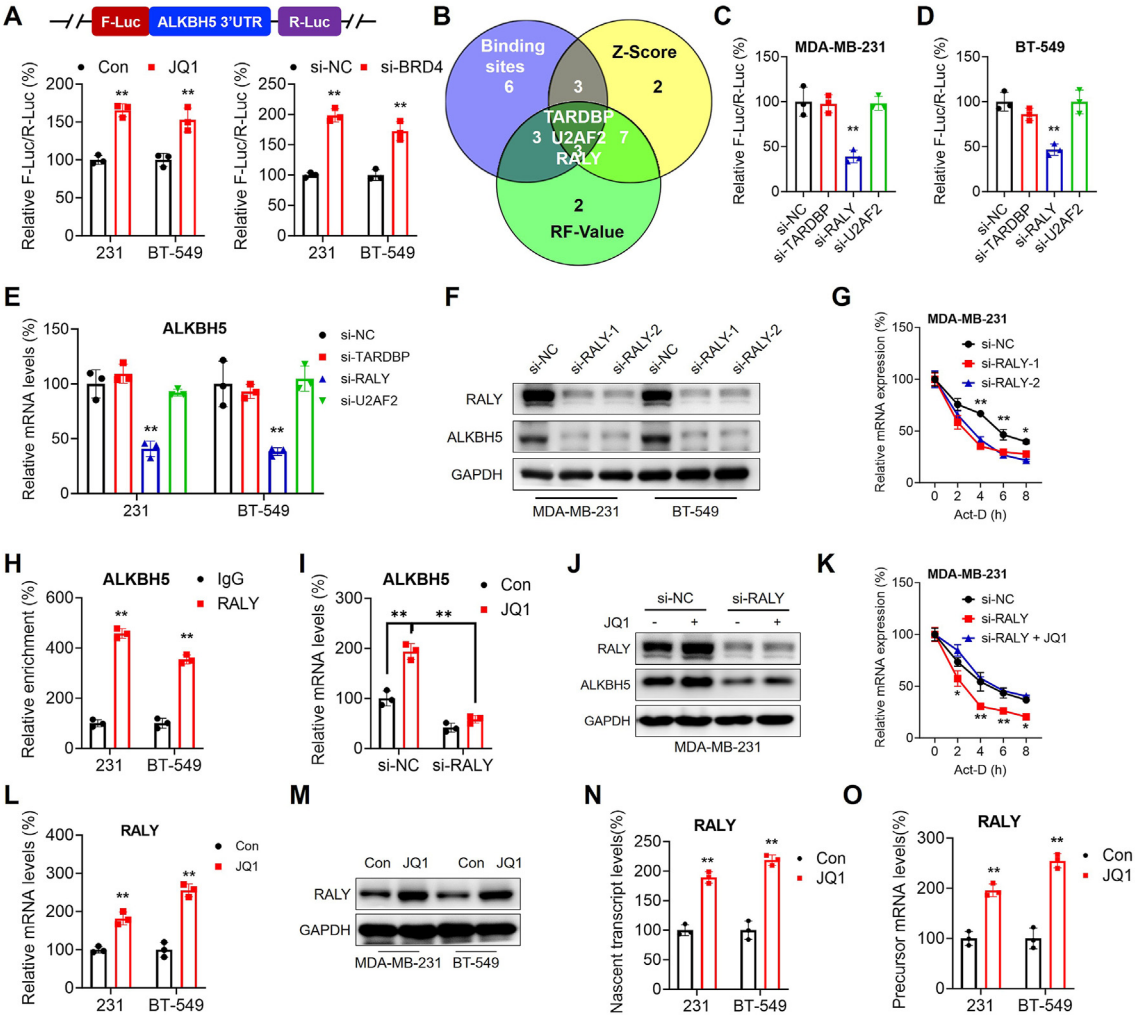

Figure 4 RALY is essential for BRD4-regulated mRNA stability of *ALKBH5*. (A) Relative luciferase activity of F-Luc/R-Luc in cells pre-transfected with pmiR-GLO-ALKBH5-3′UTR for 12 h and then further treated with or without 1 μmol/L JQ1 for 24 h, or in cells transfected with pmiR-GLO-ALKBH5-3′UTR together with si-NC or si-BRD4 for 24 h; (B) Venn diagram shows substantial and significant overlaps among the top 15 RBPs with highest binding sites, Z-score and RF-values, which were predicted by RBPmap bioinformatics program[43]; (C, D) Relative luciferase activity of F-Luc/R-Luc in MDA-MB-231 (C) or BT-549 (D) cells transfected with pmiR-GLO-ALKBH5-3′UTR together with si-NC, si-TARDBP, si-RALY, or si-U2AF2 for 24 h; (E) Relative levels of ALKBH5 mRNA in BC cells transfected with si-NC, si-TARDBP, si-RALY, or si-U2AF2 for 24 h; (F) Protein levels of ALKBH5 in cells transfected with si-NC or si-RALY for 24 h; (G) The mRNA of ALKBH5 in MDA-MB-231 cells pre-transfected with si-NC or si-RALY for 24 h and further treated with Act-D for 0−8 h; (H) Binding between RALY and *ALKBH5* mRNA was checked by ChIP-PCR using IgG or RALY antibody; (I, J) MDA-MB-231 cells were pre-transfected with si-NC or si-RALY for 12 h and further treated with or without 1 μmol/L JQ1 for 24 h. The relative mRNA (I) and protein (J) levels of ALKBH5 were checked; (K) MDA-MB-231 cells were pre-transfected with si-NC or si-RALY for 12 h and further treated with or without 1 μmol/L JQ1 for 24 h. Cells were then treated with Act-D for 0−8 h. The mRNA of *ALKBH5* was checked by qRT-PCR; (L, M) Cells were treated with or without 1 μmol/L JQ1 for 24 h. The mRNA (L) and protein (M) levels of RALY were checked; (N, O) Cells were treated with or without 1 μmol/L JQ1 for 24 h. Nascent transcripts (N) and precursor mRNA (O) of RALY were analyzed by 4sU incorporation in the newly synthesized transcripts and qPCR, respectively. Data are presented as mean ± SD from three independent experiments. $*P < 0.05$, $**P < 0.01$, ns, no significant, by Student's *t* test (two-side) as compared with the control group.

RBPs with predicted strongest binding ability, Z-Score and RF-values (Fig. 4B, Supporting Information Table S3). TARDBP, RALY, and U2AF2 were among the top hits (Fig. 4B). We then knocked down their expression using respective siRNAs (Supporting Information Fig. S3A). Our data showed that si-RALY significantly decreased pmiR-GLO-ALKBH5-3′UTR reporter activity more efficiently than that of si-TARDBP or si-U2AF2 in both MDA-MB-231 (Fig. 4C) and BT-549 (Fig. 4D) cells. In addition, si-RALY significantly decreased ALKBH5 mRNA expression in both MDA-MB-231 and BT-549 cells (Fig. 4E), again with greater efficiency than that of si-TARDBP or si-U2AF2. si-RALY also decreased the protein level (Fig. 4F) and mRNA stability of ALKBH5 in both MDA-MB-231 (Fig. 4G) and BT-549 (Fig. S3B) cells. RNA immunoprecipitation (RIP) experiments further demonstrated that RALY directly associates with ALKBH5 mRNA in BC cells (Fig. 4H), indicating that RALY might regulate the mRNA stability of ALKBH5 *via* binding to its 3′UTR.

We also investigated the role of RALY in BRD4-regulated mRNA stability and expression of ALKBH5. RALY knockdown attenuated JQ1-induced mRNA (Fig. 4I) and protein (Fig. 4J) levels of ALKBH5 in MDA-MB-231 cells. Similar results were also observed in BT-549 cells (Fig. S3C and S3D). Knockdown of RALY significantly reversed JQ1-increased mRNA half-life of ALKBH5 (Fig. 4K), indicating that RALY is involved in BRD4-regulated expression and mRNA stability of ALKBH5.

We also investigated the effects of BRD4 on the expression of RALY. Our data showed that JQ1 increased the mRNA expression of RALY in BC cells (Fig. 4L). Consistently, increased protein expression of RALY was also observed in JQ1-treated BC cells (Fig. 4M). In addition, si-BRD4 also increased the mRNA (Fig. S3E) and protein (Fig. S3F) expression of RALY in BC cells. This might be due to JQ1-increased transcription of RALY, since JQ1 treatment could increase the nascent transcript checked by

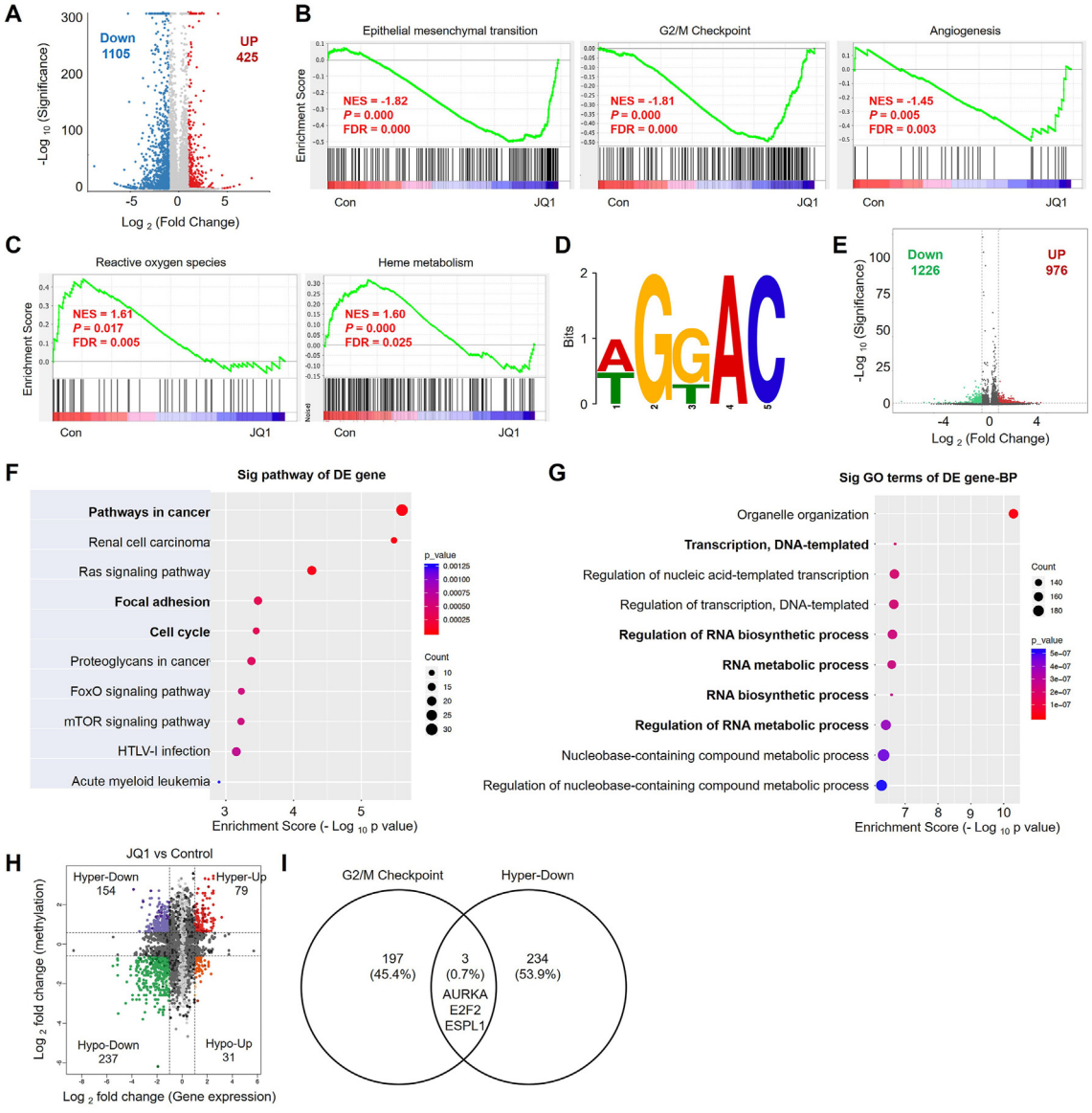

Figure 5 Variation of epi-transcriptome and transcriptome in BC cells treated with JQ1. (A) Scatter plot of differential expression of mRNAs assessed from RNA-seq data in MDA-MB-231 cells treated with or without 1 μmol/L JQ1 for 24 h. Red dots denote upregulated genes and green dots denote downregulated genes; (B) GSEA reveals negative enrichment of JQ1-altered genes in EMT, G2/M checkpoint, and angiogenesis gene sets; (C) GSEA reveals positive enrichment of JQ1-altered genes in reactive oxygen species and heme metabolism gene sets; (D) Predominant consensus motif GGAC was detected in m^{6}A-seq; (E) Volcano plots to determine different m^{6}A peaks in MDA-MB-231 cells treated with or without 1 μmol/L JQ1 for 24 h. The *x*-axis represents log2-fold changes (FC) of peaks and the y-axis represents the −log10 of the *P*-values for the various condition pairs. Each dot represents a peak; (F) Cluster profiler identifies the enriched KEGG processes for assembled peaks of the transcriptome decreased in JQ1-treated cells compared with control cells; (G) Cluster profiler identifies the enriched gene ontology processes for assembled peaks of the transcriptome decreased in JQ1-treated cells compared with control cells; (H) Correlation between the levels of gene expression (overall transcript) and changes in m^{6}A levels in JQ1-treated cells compared with control cells; (I) Venn diagram shows substantial and significant overlaps among the m^{6}A downregulated genes, JQ1-decreased genes, and G2/M checkpoint genes.

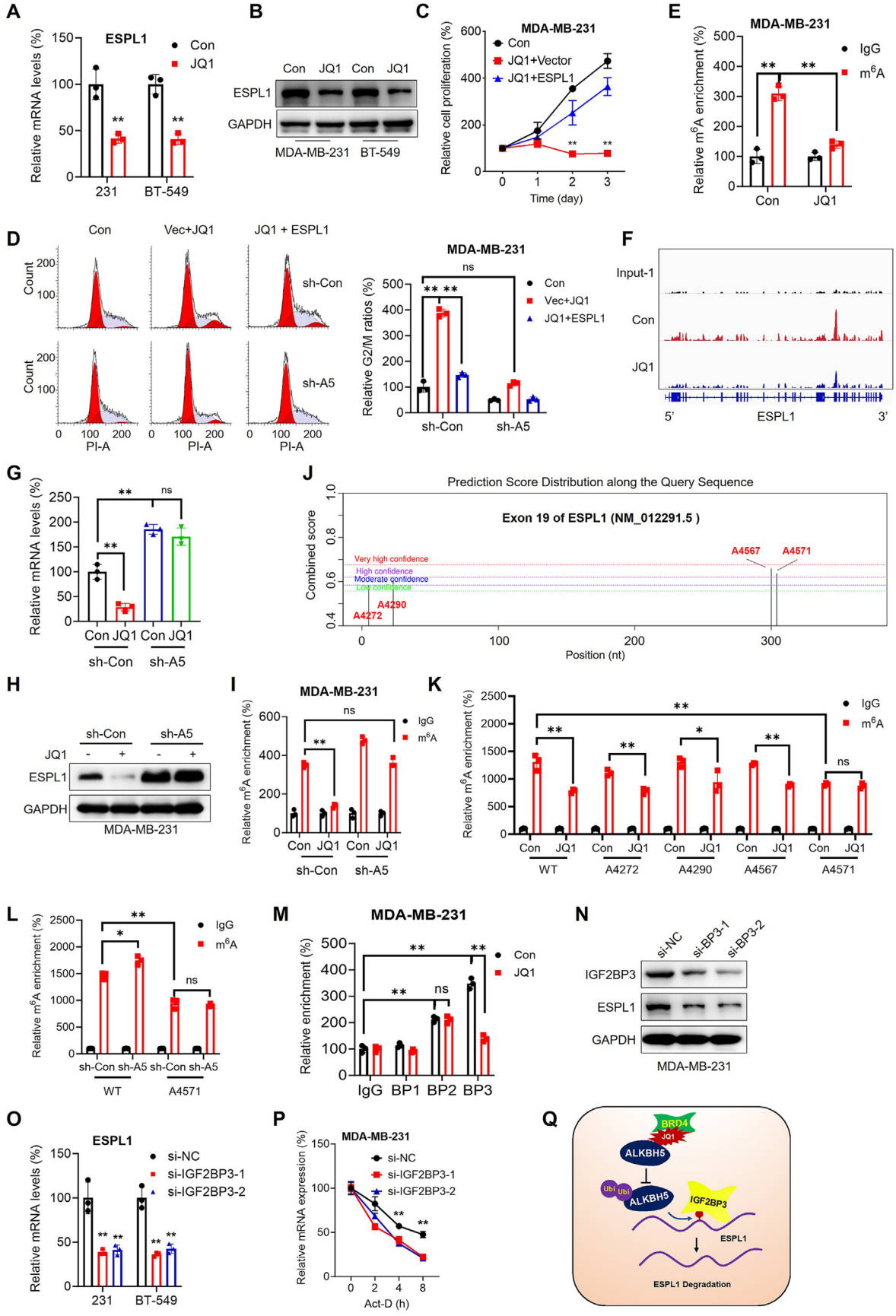

Figure 6 ESPL1 is an effector for BRD4/ALKBH5 axis-regulated cell cycle progression. (A, B) Cells were treated with or without 1 μmol/L JQ1 for 24 h. The mRNA (A) and protein (B) levels of ESPL1 were checked; (C) Cell proliferation of MDA-MB-231 cells pre-transfected with

4sU-labelling (Fig. 4N) and precursor mRNA (Fig. 4O) as checked by qRT-PCR using primer spanning the exon 1 and intron 2 of RALY1. Taken together, these experiments validate that RALY is involved in BRD4-regulated mRNA stability of ALKBH5.

3.5. *Variation of epi-transcriptome and transcriptome in BC cells treated with JQ1*

To characterize downstream effectors involved in BRD4-regulated malignancy of BC cells, we performed mRNA-seq in MDA-MB-231 cells treated with or without JQ1. The expression levels of 1530 genes were found to be significantly changed with upregulation of 425 and downregulation of 1105 genes in JQ1-treated cells (Fig. 5A, Supporting Information Table S4). Individually sequenced transcriptomes and differentially expressed genes in cells treated with or without JQ1 are indicated in Supporting Information Fig. S4A. Gene Set Enrichment Analysis (GSEA) revealed that the JQ1 treatment gene expression profile was negatively associated with EMT, G2/M checkpoint, and angiogenesis (Fig. 5B). In addition, it positively associated with reactive oxygen species and heme metabolism (Fig. 5C). The transcriptome study revealed that JQ1 treatment suppresses gene expression, cell proliferation, wound closure and migration of BC cells.

We also mapped m^6A methylomes of MDA-MB-231 cells treated with or without JQ1 to identify genes involved in BRD4-regulated RNA methylation. Sequence analysis of m^6A peaks showed that the GGAC motif is highly enriched within m^6A sites in the cell (Fig. 5D). m^6A-seq analysis identified 27,206 and 26,956 m^6A peaks from 7679 to 7240 m^6A-modified transcripts in cells treated with or without JQ1, respectively (Supporting Information Table S5). In JQ1-treated cells, 976 increased and 1226 decreased m^6A transcripts were observed (Fig. 5E). Similar patterns of total m^6A distributions in cells treated with or without JQ1 were observed (Fig. S4B), showing that m^6A peaks were predominantly distributed in coding sequences (CDSs), 3′UTRs, and near stop codons. KEGG (Kyoto Encyclopedia of Genes and Genomes) analysis showed that m^6A modification in JQ1-downregulated genes are mainly involved in cancer, cell cycle and adhesion pathways (Fig. 5F), and as identified by Gene Ontology (GO) analysis of biological processes (BP) also in regulation of transcription, RNA biosynthetic and metabolic processes (Fig. 5G). Collectively, the m^6A-seq data indicated that a handful of m^6A modified genes were associated with cell malignancy and RNA dynamics in BC cells.

We classified upregulated peaks as hypermethylated m^6A peaks and downregulated peaks as hypomethylated m^6A peaks. To correlate the gene expression level with the m^6A modification level, we plotted the m^6A peak data against the RNA-seq data of gene expression (Fig. 5H and Supporting Information Table S6). Given that JQ1 induced the expression of ALKBH5, which then led to a decrease in global m^6A levels, we predicted that mRNA transcripts carrying hypomethylated m^6A peaks, including hypo-down and hypo-up genes, are likely to be potential targets of JQ1 (Supporting Information Table S7). Overlap analysis identified 31 hypo-up and 237 hypo-down genes (Fig. 5H).

Since both cell cycle analysis and GESA revealed that JQ1 could induce G2/M cell cycle arrest, we further checked the m^6A-regulated genes involved in BRD4-regulated cell cycle progression. Among the 200 G2/M checkpoint-related genes (Supporting Information Table S8), three genes (AURKA, E2F2, and ESPL1) were overlapped with 237 hypo-down genes (Fig. 5I), indicating that these genes might be involved in BRD4/ALKBH5 axis-regulated malignancy of BC cells.

3.6. *ESPL1 is an effector for BRD4/ALKBH5 axis-regulated cell cycle progression*

Since overlap analysis showed that AURKA (Aurora Kinase A), E2F2 (E2F Transcription Factor 2), and ESPL1 might be involved in BRD4/ALKBH5 axis-regulated BC progression, we further checked the effects of JQ1 on their expression. Our data suggested that JQ1 treatment significantly decreased the mRNA levels of AURKA, E2F2, and ESPL1 in MDA-MB-231 cells (Supporting Information Fig. S5A), and the decreased fold of ESPL1 was greatest among the three genes. Similar results were obtained for the protein levels of AURKA, E2F2, and ESPL1 (Fig. S5B), with a lesser decrease of both AURKA and E2F2 compared with that of mRNAs likely due to compensatory effects incurred during translation or post-translation. We therefore focused on the

vector control or ESPL1 construct for 12 h were then further treated with or without 1 μmol/L JQ1 for 1−3 days; (D) MDA-MB-231 cells were synchronized at the G1/S transition by a double TdR block and then transfected with vector control or ESPL1 construct for 12 h and then further treated with or without 1 μmol/L JQ1 for 24 h. The cell cycles were analyzed by flow cytometry (FCM); (E) The m^6A levels of ESPL1 in MDA-MB-231 cells treated with or without 1 μmol/L JQ1 for 24 h were checked by m^6A-RIP-PCR; (F) m^6A peaks were decreased in *ESPL1* mRNA in JQ1-treated MDA-MB-231 cells from m^6A RIP-seq data; (G, H) The mRNA (G) and protein (H) expression of ESPL1 in sh-Control or sh-ALKBH5 MDA-MB-231 cells treated with or without 1 μmol/L JQ1 for 24 h; (I) The m^6A levels of ESPL1 in sh-Control or sh-ALKBH5 MDA-MB-231 cells treated with or without 1 μmol/L JQ1 for 24 h; (J) The predicted m^6A peaks in *ESPL1* mRNA from the m^6A sites predictor SRAMP; (K) MDA-MB-231 cells were transfected with either wild-type ESPL1 overexpression plasmids or plasmids with mutated predicted m^6A sites ("A" to "C") for 24 h. After treating JQ1 for another 24 h, the m^6A modification levels of *ESPL1* mRNA was detected using m^6A-RIP-qPCR; (L) After transfecting MDA-MB-231 cells with either wild-type ESPL1 overexpression plasmids or plasmids with mutated A4571 sites for 24 h, the m^6A modification levels of *ESPL1* mRNA was detected using m^6A-RIP-qPCR; (M) MDA-MB-231 cells were treated with or without 1 μmol/L JQ1 for 24 h. The relative binding between *ESPL1* mRNA and IGF2BPs was checked by RIP-PCR using antibodies of IGF2BP1/2/3, respectively; (N, O) The protein (N) and mRNA (O) expression of ESPL1 in cells transfected with si-NC or si-IGF2BP3 for 24 h; (P) The mRNA of *ESPL1* in MDA-MB-231 cells pre-transfected with si-NC or si-IGF2BP3 for 24 h and further treated with Act-D for 0−8 h; (Q) Proposed model for mechanistic action of ESPL1 as an effector for BRD4/ALKBH5 axis-regulated cell cycle progression. JQ1 inhibits the binding of BRD4 to ALKBH5, leading to a reduction in ALKBH5 ubiquitination levels and an upregulation of ALKBH5 expression. ALKBH5 recognizes and binds to *ESPL1* mRNA m^6A through IGF2BP3, thereby removing the m^6A modification on *ESPL1* mRNA, ultimately resulting in the degradation of *ESPL1* mRNA. Data are presented as mean ± SD from three independent experiments. $*P < 0.05$, $**P < 0.01$, ns, no significant, by Student's *t* test (two side). Fig. 6I and J were analyzed by one-way ANOVA followed by Bonferroni test.

potential role of ESPL1 in BRD4/ALKBH5 axis-regulated BC progression.

ESPL1, an endopeptidase activated at the onset of anaphase, has been suggested as the top gene of oncogenic drivers for breast cancer[44−46]. Our data showed that JQ1 treatment decreased the mRNA (Fig. 6A) and protein (Fig. 6B) levels of ESPL1 in both MDA-MB-231 and BT-549 cells. Consistently, si-BRD4 also decreased the mRNA (Fig. S5C) and protein (Fig. S5D) levels of ESPL1 in BC cells. However, JQ1 had no significant effect on the precursor mRNA (Fig. S5E) or nascent transcript (Fig. S5F) of ESPL1 in MDA-MB-231 and BT-549 cells, which suggested that JQ1 had no effect on the transcription of ESPL1 in BC cells.

We further evaluated whether ESPL1 is essential for BRD4-regulated malignancy of cancer cells. Our data showed that overexpression of ESPL1 (Fig. S5G) attenuated JQ1-suppressed proliferation of MDA-MB-231 (Fig. 6C) and BT-549 (Fig. S5H) cells. In addition, overexpression of ESPL1 rescued JQ1-inducd G2/M cell cycle arrest of MDA-MB-231 cells (Fig. 6D). Further, overexpression of ESPL1 can also restore JQ1-suppressed colonization of both MDA-MB-231 and BT-549 cells (Fig. S5I). However, over expression of ESPL1 had no effect on the protein expression of BRD4 or ALKBH5 in BC cells (Fig. S5G). These results indicated that ESPL1 is a downstream effector for BRD4-regualted proliferation and cell cycle progression in BC cells.

We further investigated whether ALKBH5/m^{6}A is essential for BRD4-regulated expression of ESPL1. Overexpression of ALKBH5, while not the catalytically dead ALKBH5 H204A mutant, suppressed the mRNA (Fig. S5J) and protein (Fig. S5K) levels of ESPL1 in BC cells. m^{6}A-RIP-PCR confirmed that *ESPL1* mRNA was m^{6}A-modified. However, JQ1 treatment significantly decreased the m^{6}A level of *ESPL1* mRNA in MDA-MB-231 (Fig. 6E) and BT-549 (Fig. S5L) cells, which was further confirmed by m^{6}A-RIP-seq in MDA-MB-231 cells (Fig. 6F). Knockdown of ALKBH5 attenuated JQ1-suppressed mRNA and protein levels of ESPL1 in MDA-MB-231 (Fig. 6G and H) and BT-549 (Fig. S5M) cells, likely due to ALKBH5 knockdown attenuating JQ1-suppressed m^{6}A levels of *ESPL1* mRNA in both MDA-MB-231 (Fig. 6I) and BT-549 (Fig. S5N) cells. Further, m^{6}A-RIP-PCR analysis showed that overexpression of HDAC2 (Fig. S5O) or knockdown of TRIM21 (Fig. S5P) significantly decreased the m^{6}A levels of *ESPL1* mRNA in MDA-MB-231 cells, while knockdown of RALY (Fig. S5Q) significantly increased the m^{6}A levels of ESPL1 mRNA.

Using the m^{6}A site prediction tool SRAMP (http://www.cuilab.cn/sramp), we predicted four potential m^{6}A modification sites within exon 19 of *ESPL1* mRNA (Fig. 6J). We mutated these four predicted sites ("A" to "C") and then performed m^{6}A-RIP-qPCR experiments. The results indicated that mutation at site A4571 significantly reduced the m^{6}A modification of ESPL1 and attenuated JQ1-suppressed m^{6}A levels of *ESPL1* mRNA (Fig. 6K). Further, we transfected a plasmid with a mutated A4571 site into ALKBH5 knockdown MDA-MB-231 cells. The results showed that the A4571 mutation significantly reduced the m^{6}A modification of *ESPL1* mRNA and attenuated ALKBH5-knockdown-suppressed m^{6}A levels of *ESPL1* mRNA (Fig. 6L). These findings imply that A4571 may serve as a pivotal regulatory m^{6}A modification site on *ESPL1* mRNA.

Since overexpression of ALKBH5 suppressed the mRNA of *ESPL1*, we investigated the roles of m^{6}A reader proteins IGF2BP1/2/3, which can bind and stabilize m^{6}A-methylated mRNA[33], in m^{6}A-regulated expression of ESPL1. After pulldown of IGF2BP1/2/3, results of RIP-PCR showed that both IGF2BP2 and IGF2BP3, but not IGF2BP1, bind ESPL1 mRNA in MDA-MB-231 (Fig. 6M) and BT-549 (Fig. S5R) cells. JQ1 only decreased *ESPL1* mRNA binding with IGF2BP3, but not with IGF2BP2 (Fig. 6M and Fig. S5R). When IGF2BP3 was knocked down in MDA-MB-231 cells, ESPL1 protein (Fig. 6N) and mRNA (Fig. 6O) levels were correspondingly reduced, potentially due to si-IGF2BP3-decreased mRNA stability of *ESPL1* (Fig. 6P). These results indicate that BRD4/ALKBH5 might regulate ESPL1 expression though IGF2BP3-stabilized m^{6}A-methylated mRNA (Fig. 6Q).

3.7. *BRD4/ALKBH5/ESPL1 axis regulating in vivo BC progression*

We further investigated the potential roles of the BRD4/ALKBH5/ESPL1 axis in BC *in vivo* progression. Firstly, we checked their expression in our breast cancer cell models with high lung metastasis potential, previously named as MDA-MB-231^{LMF3} and BT549^{LMF3} cells[34]. Increased expression of BRD4 and ESPL1, associated with decreased expression of ALKBH5, was observed in MDA-MB-231^{LMF3} (Fig. 7A) and BT549^{LMF3} (Supporting Information Fig. S6A) cells compared to their parental control cells. Western blot analysis confirmed decreased ALKBH5, accompanied by increased BRD4 and ESPL1, in high lung metastasis potential cancer cells (Fig. 7B). Metastasized lung tumors and primary breast tumors were isolated from the mouse mammary tumor virus-polyoma middle tumor-antigen (MMTV-PyMT) mice. qRT-PCR (Fig. S6B) and Western blot analysis (Fig. S6C) showed enhanced expression of BRD4 and ESPL1 with decreased expression of ALKBH5 in metastasized lung tumors compared to those in the primary tumors isolated from MMTV-PyMT mice.

In xenografts from mice implanted with a triple-negative breast cancer (TNBC) patient dependent xenograft (PDX) model treated with vehicle or JQ1[29], immunohistochemistry (IHC) data showed that JQ1 increased the expression of ALKBH5 while decreasing the expression of ESPL1 in the PDX model (Fig. 7C). To test the *in vivo* effects of ALKBH5 in BRD4-mediated BC progression, we implanted mice with sh-Con or sh-ALKBH5 MDA-MB-231 cells and further treated with vehicle or JQ1. Results showed that JQ1 treatment significantly inhibited the growth of MDA-MB-231 xenografts (Fig. 7D). At the end of the experiment, tumor size (Fig. 7E), volume (Fig. 7F), and weight (Fig. 7G) in the JQ1-injected MDA-MB-231 group were significantly lower than those measured in the sh-control MDA-MB-231 group. sh-ALKBH5 increased the tumor size, volume and weight more significantly than that of the sh-control MDA-MB-231 group and reversed JQ1-suppressed tumor size, volume and weight (Fig. 7D−G). No significant change of body weight was observed among all groups (Fig. S6D). Further, Ki67-positive staining, which recognizes a nuclear antigen expressed in proliferating cells, in the JQ1 group was decreased *in vivo*, while sh-ALKBH5 abolished JQ1-suppressed expression of Ki67 (Fig. 7H). IHC data confirmed that knockdown of ALKBH5 abolished JQ1-suppressed expression of ESPL1 (Fig. 7I), indicating that BRD4/ALKBH5 could regulate the *in vivo* growth of xenografts and expression of EPSL1.

We then analyzed expression of the axis components and their correlation with clinical characteristics of BC. The expression of ALKBH5 in normal tissue was significantly greater than that in the tumor tissue according to Finak (Fig. 7J), Perou (Fig. S6E), and Turashvili (Fig. S6F) breast data from the Oncomine database. While the expression of BRD4 (Fig. 7K) and ESPL1 (Fig. 7L) in

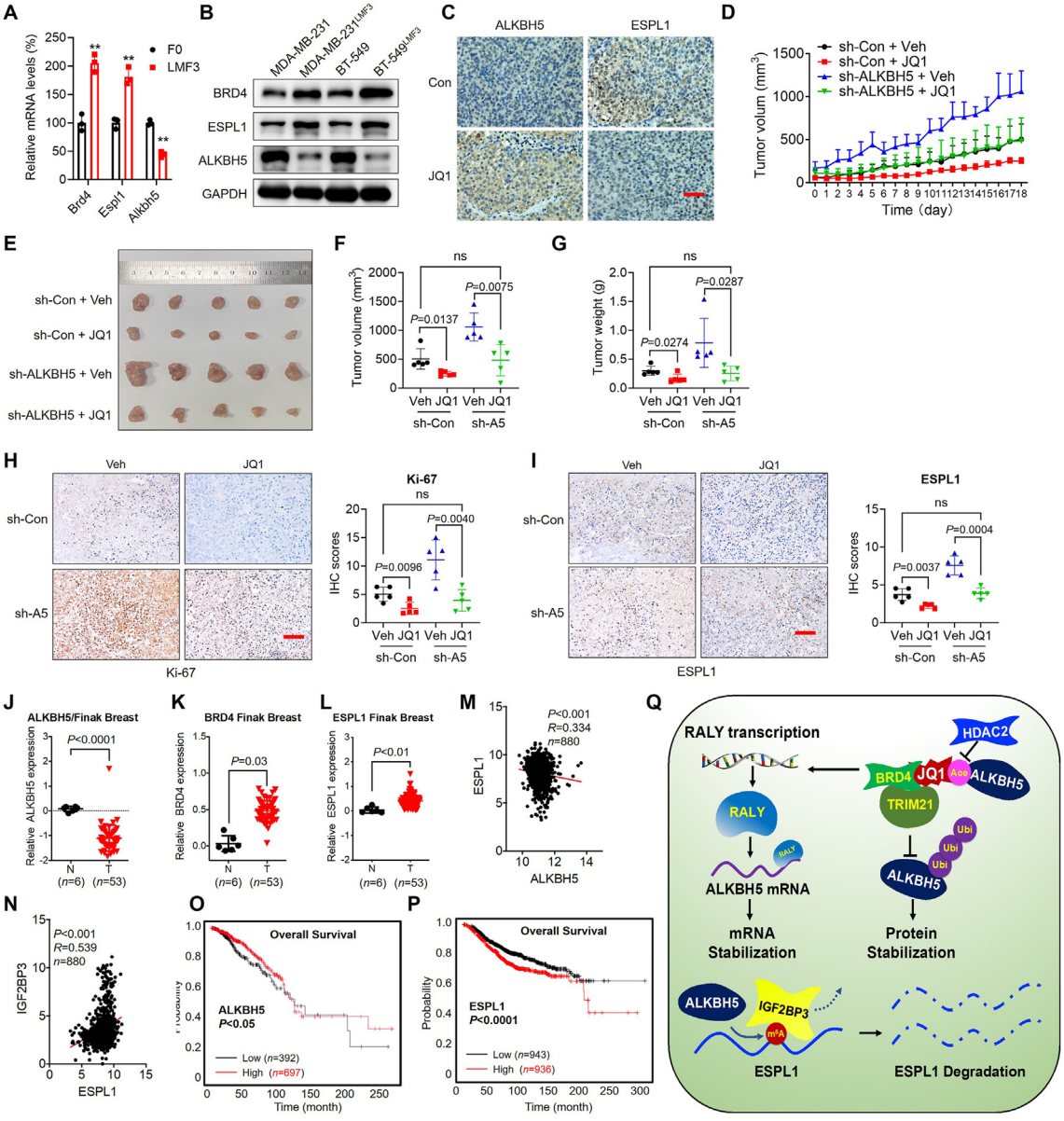

Figure 7 BRD4/ALKBH5/ESPL1 axis regulating the progression of BC. (A) The mRNA expression of *BRD4*, *EPSL1*, and *ALKBH5* was measured in MDA-MB-231^{LMF3} and F0 xenograft tumor tissues by qRT-PCR; (B) The protein expression of BRD4, EPSL1, and ALKBH5 was measured in MDA-MB-231^{LMF3}, BT-549^{LMF3}and their F0 xenograft tumor tissues by Western blot analysis; (C) IHC (ALKBH5 and ESPL1)-stained paraffin-embedded sections obtained from patient-derived tumors treated with or without JQ1, scale bar: 100 μm; (D) Tumor growth curves of mice were xenografts implanted with sh-Con and sh-ALKBH5 MDA-MB-231 cells and further treated with vehicle or JQ1 at indicated time intervals; (E−G) Tumor images (E), volumes (F) and weights (G) of xenografts implanted with sh-Con and sh-ALKBH5 MDA-MB-231 cells and further treated with vehicle or JQ1; (H, I) IHC (Ki-67 and ESPL1)-stained paraffin-embedded sections obtained from xenografts (left) and quantitatively analyzed (right), scale bar: 200 μm; (J−L) The relative mRNA expression of *ALKBH5* (J), *BRD4* (K), and *ESPL1* (L) in BC tumor tissue (T) and normal tissue (N) from Oncomine database; (M, N) Correlation of *ESPL1* mRNA with ALKBH5 (M) or IGF2BP3 (N) in 880 breast cancer tissues from the TCGA database; (O, P) Overall survival (OS) in patients with high *vs.* low levels of ALKBH5 (O) or ESPL1 (P) in BC patients plotted by the Kaplan−Meier method; (Q) Proposed model to illustrate the mechanisms of BRD4/ALKBH5/ESPL1 axis-regulated BC progression. BRD4 regulates ALKBH5 expression through two pathways. Firstly, JQ1 inhibition of BRD4 reduces the binding of TRIM21 to ALKBH5, decreasing the ubiquitination of ALKBH5 by TRIM21, which in turn increases the stability of ALKBH5 protein. HDAC2 can also regulate ALKBH5 protein stability by affecting its acetylation. Secondly, inhibiting BRD4 can increase the transcription level of RALY. RALY binds to the 3′ UTR of *ALKBH5* mRNA, increasing its stability. Consequently, inhibiting BRD4 upregulates ALKBH5 levels. ALKBH5 recognizes and binds to *ESPL1* mRNA m^{6}A through IGF2BP3, thereby removing the m^{6}A modification on *ESPL1* mRNA, ultimately leading to the degradation of *ESPL1* mRNA and influencing the progression of breast cancer. Data are presented as mean ± SD from three independent experiments. *$P < 0.01$, **$P < 0.05$, ns, no significant, by Student's *t* test (two-side). Fig. 7F−I was analyzed by one-way ANOVA followed by Bonferroni test.

tumor tissue were significantly greater than that in normal tissue according to the Finak breast data from the Oncomine database. In the TCGA dataset, the expression of BRD4 (Fig. S6G) and ESPL1 (Fig. S6H) in tumor tissue were significantly greater than that in normal tissue), while no significant difference in expression of ALKBH5 (Fig. S6I). Expression of ALKBH5 in ERα (Fig. S6J) and PR (Fig. S6K)-negative BCs was significantly ($P < 0.05$) less than those in their corresponding-positive BCs. The expression of ALKBH5 was also decreased in Grades 2 and 3 BCs as compared with that in Grade 1 BC (Fig. S6L). In addition, the expression of ALKBH5 was decreased in TP53-positive (Fig. S6M) and TP53 mutant (Fig. S6N) BCs as compared with those in their corresponding controls. All these data showed that ALKBH5 has anti-oncogenic effects and is negatively associated with BC progression.

The data from LinkedOmics showed expression of ESPL1 negatively correlated ($P < 0.05$) with the expression of ALKBH5 (Fig. 7M) but positively correlated with the expression of IGF2BP3 (Fig. 7N) in 880 BC patients, suggesting an *in vivo* correlation of the ALKBH5/ESPL1 axis with disease progression. The expression of ALKBH5 mRNA was negatively correlated with the expression of proliferating cell nuclear antigen (PCNA) (Fig. S6O) and cyclin B2 (CCNB2) (Fig. S6P) in BC tissues. Further, the expression of ALKBH5 mRNA was negatively correlated with the EMT-transcription factors including Snail (Fig. S6Q), Slug (Fig. S6R), Twist1 (Fig. S6S), ZEB1 (Fig. S6T), and mesenchymal markers including MMP2 (Fig. S6U), and FN1 (Fig. S6V). Using online bioinformatics tool Kaplan−Meier plotter[47], we found BC patients with increased expression of ALKBH5 had significantly increased OS (Fig. 7O). Further, BC patients with increased expression of ESPL1 showed significantly reduced OS (Fig. 7P). Altogether, these results suggest the BRD4/ALKBH5/ESPL1 axis could trigger the progression of BC.

4. Discussion

In this study, we examined the biological effects of targeted inhibition of BRD4 on m^{6}A modification and BC progression (Fig. 7Q). Our results showed that targeted inhibition of BRD4 decreased mRNA m^{6}A and suppressed the malignancy of BC cells by increasing the expression of ALKBH5, an important demethylase for mRNA methylation. We found that inhibition of BRD4 by siRNA or a BET inhibitor (JQ1) increased the mRNA stability of ALKBH5 *via* enhancing the binding between ALKBH5 3′UTR with RALY. Further, BRD4 could serve as scaffold for ubiquitin enzyme TRIM21 and ALKBH5, resulting in the ubiquitination and degradation of ALKBH5 protein. JQ1-increased ALKBH5 demethylates mRNA of ESPL1, a critical oncogenic driver for breast cancer, which leads to reduced binding between ESPL1 mRNA and m^{6}A reader IGF2BBP3 and decay of ESPL1 mRNA. Animal and clinical studies confirmed the BRD4/ALKBH5/ESPL1 pathway is critical for BC progression.

Our study revealed for the first time that BRD4 regulates mRNA m^{6}A *via* regulation of ALKBH5. Although many studies have shown the importance of BRD4 on histone acetylation and transcriptional regulation[4,48−50], few have shown non-canonical, non-transcriptional functions of BRD4 and their implications in cancer biology[51]. It has been found that BRD4 reading of the chromatin state and its involvement in chromatin organization are critical for DNA damage repair[52−54] and telomere maintenance *via* regulation of Telomerase Reverse Transcriptase (TERT) expression[55]. BRD4 recruits transcription factors such as positive transcription elongation factor b (P-TEFb) and nuclear factor-κB (NF-κB)[56]. m^{6}A RNA methylation has crucial roles in RNA metabolism. Recent studies suggest that RNA m^{6}A serves as a scaffold for association with specialized RNA-binding proteins to regulate chromatin state and local transcription[25,26,57]. Our present study shows that BRD4 can influence nascent RNA methylation and metabolism in cancer cells.

We found that inhibition of BRD4 increases the mRNA and protein stability of ALKBH5. JQ1 treatment increased the binding between ALKBH5 mRNA 3′UTR with RALY, thus stabilizing the mRNA of ALKBH5, which occurs in the nucleus. RALY is a member of the hnRNPs family reported to regulate the stability of specific transcripts. RALYL binds 3′-UTR of transforming growth factor (TGF)-β2 mRNA to increase hepatocellular carcinoma stemness[58]. In our finding, BRD4 serves as scaffold for ubiquitin enzyme TRIM21 and ALKBH5, and JQ1 decreased this interaction and ubiquitination of ALKBH5 to increase its expression. BRD4 inhibitors, such as I-BET, JQ1, and MS417, are acetyl-lysine mimics to prevent the interaction between BRD4 and acetyl-lysine by competitively binding to BRD4[59]. For example, JQ1 inhibits the binding of BRD4 to the *C-MYC* locus to suppress cancer progression[60]. Our study revealed that JQ1 also suppresses the interaction between BRD4 and ALKBH5, resulting in decrease of TRIM21-mediated ubiquitination and upregulation of ALKBH5 protein stability. The degradation of ALKBH5 proteins through the UPS (ubiquitin-proteasome system) occurs in the cytoplasm. Therefore, our findings also suggest that BRD4 exerts dual regulatory roles in both the nucleus and cytoplasm, corresponding to the regulation of mRNA and protein stability of ALKBH5, respectively.

Our data showed that ESPL1, a critical oncogenic driver for breast cancer, was involved in BRD4/ALKBH5-regulated BC progression. Mechanistically, JQ1-increased ALKBH5 can demethylate mRNA of ESPL1, which suppresses the binding between ESPL1 mRNA and m^{6}A reader IGF2BP3 and facilitates the decay of ESPL1 mRNA. ESPL1 is introduced to mitotic chromosomes to dissolve the cohesion of the sister chromatid in a DNA-dependent manner[61]. It is overexpressed and acts as an important oncogene in several types of breast cancers[62]. Analysis of the cancer genome atlas (TCGA) dataset indicated that more than 53% of breast tumors overexpress *ESPL1* transcript[63]. However, the mechanisms responsible for the upregulation of ESPL1 have not been reported. Our results indicated that m^{6}A methylation-induced mRNA stability might be responsible for upregulation of ESPL1 in BC cells and tissues.

5. Conclusions

Our study shows that BRD4 can modulate RNA m^{6}A methylation and BC progression *via* regulation of ALKBH5. Although many studies have shown the importance of ALKBH5[64,65], few have shown how the demethylase complex itself is regulated. It has been revealed that m^{6}A methylation can enhance the translation of oncogenic BRD4 through forming an mRNA loop with eukaryotic initiation factor 3 (eIF3)[66], indicating a positive feedback loop between BRD4 and ALKBH5. It would be interesting to explore how histone modification and nascent RNA methylation may coordinate with each other to promote cancer progression.

Acknowledgements

We thank Prof. Jiemin Wong at the East China Normal University for the HDAC2 plasmid. This research was supported by the

National Key Research and Development Program of China (No. 2022YFC2601800), the National Natural Science Foundation of China (Nos. 82472761, 32161143017, 82173833, 82372743, 82173126, 82373893, 82341053, and 32100584), the Guangdong Basic and Applied Basic Research Foundation (Nos. 2023B1515040006, China), the Key-Area Research and Development Program of Guangdong Province (No. 2023B1111020007, China), the Guangzhou Science and Technology Program (No. 2024A04J6480, China), the Guangdong Provincial Key Laboratory of Construction Foundation (No. 2023B1212060022, China), the Shenzhen Bay Scholars Program, the Natural Science Foundation of Shandong Province (No. ZR2021QC061, China), the Natural Science Foundation of Hunan Province of China (No. 2022JJ40413), the Outstanding Youth Project of Hunan Provincial Department of Education (No. 22B0814, China), the Young Teachers Cultivation Program of Basic Research Operating Expenses of Universities at Sun Yat-sen University (No. 23qnpy117, China), the Research Project of TCM Bureau of Guangdong Province (No. 20231324, China), the Special Fund of Foshan Climbing Peak Plan (No. 2020B018, China), and the Basic and Applied Basic Research Foundation of Guangdong Province (No. 2022A1515140091, China).

Author contributions

Haisheng Zhang: Writing − review & editing, Writing − original draft, Methodology, Investigation, Formal analysis, Data curation, Conceptualization. Linlin Lu: Writing − original draft, Data curation. Cheng Yi: Visualization, Validation, Funding acquisition. Tao Jiang: Writing − original draft, Investigation, Data curation. Yunqing Lu: Investigation, Formal analysis, Data curation. Xianyuan Yang: Methodology, Investigation. Ke Zhong: Investigation, Data curation. Jiawang Zhou: Visualization, Validation, Data curation. Jiexin Li: Writing − review & editing, Writing − original draft. Guoyou Xie: Validation, Software. Zhuojia Chen: Writing − review & editing, Writing − original draft. Zongpei Jiang: Writing − review & editing, Writing − original draft. Gholamreza Asadikaram: Resources, Investigation. Yanxi Peng: Writing − original draft, Resources. Dan Zhou: Writing − review & editing, Writing − original draft, Resources. Hongsheng Wang: Writing − review & editing, Writing − original draft, Funding acquisition, Formal analysis, Data curation, Conceptualization.

Conflicts of interest

The authors declare no conflicts of interest.

Appendix A. Supporting information

Supporting information to this article can be found online at https://doi.org/10.1016/j.apsb.2024.12.037.

References

1. Bradner JE, Hnisz D, Young RA. Transcriptional addiction in cancer. *Cell* 2017;**168**:629−43.
2. Hammond CM, Stromme CB, Huang H, Patel DJ, Groth A. Histone chaperone networks shaping chromatin function. *Nat Rev Mol Cell Biol* 2017;**18**:141−58.
3. Wu SY, Chiang CM. The double bromodomain-containing chromatin adaptor Brd4 and transcriptional regulation. *J Biol Chem* 2007;**282**:13141−5.
4. Wu SY, Lee CF, Lai HT, Yu CT, Lee JE, Zuo H, et al. Opposing functions of BRD4 isoforms in breast cancer. *Mol Cell* 2020;**78**:1114−32.
5. Chiang CM. Brd4 engagement from chromatin targeting to transcriptional regulation: selective contact with acetylated histone H3 and H4. *F1000 Biol Rep* 2009;**1**:98.
6. Kanno T, Kanno Y, LeRoy G, Campos E, Sun HW, Brooks SR, et al. BRD4 assists elongation of both coding and enhancer RNAs by interacting with acetylated histones. *Nat Struct Mol Biol* 2014;**21**:1047−57.
7. Dai X, Gan W, Li X, Wang S, Zhang W, Huang L, et al. Prostate cancer-associated SPOP mutations confer resistance to BET inhibitors through stabilization of BRD4. *Nat Med* 2017;**23**:1063−71.
8. Asangani IA, Dommeti VL, Wang X, Malik R, Cieslik M, Yang R, et al. Therapeutic targeting of BET bromodomain proteins in castration-resistant prostate cancer. *Nature* 2014;**510**:278−82.
9. Spriano F, Stathis A, Bertoni F. Targeting BET bromodomain proteins in cancer: the example of lymphomas. *Pharmacol Ther* 2020:107631.
10. Andrieu G, Belkina AC, Denis GV. Clinical trials for BET inhibitors run ahead of the science. *Drug Discov Today Technol* 2016;**19**:45−50.
11. Tang P, Zhang J, Liu J, Chiang CM, Ouyang L. Targeting bromodomain and extraterminal proteins for drug discovery: from current progress to technological development. *J Med Chem* 2021;**64**:2419−35.
12. Shi J, Vakoc CR. The mechanisms behind the therapeutic activity of BET bromodomain inhibition. *Mol Cell* 2014;**54**:728−36.
13. Frye M, Harada BT, Behm M, He C. RNA modifications modulate gene expression during development. *Science* 2018;**361**:1346−9.
14. Liu JZ, Yue YN, Han DL, Wang X, Fu Y, Zhang L, et al. A METTL3−METTL14 complex mediates mammalian nuclear RNA *N*-6-adenosine methylation. *Nat Chem Biol* 2014;**10**:93−5.
15. Jia G, Fu Y, Zhao X, Dai Q, Zheng G, Yang Y, et al. N^6-Methyladenosine in nuclear RNA is a major substrate of the obesity-associated FTO. *Nat Chem Biol* 2011;**7**:885−7.
16. Zheng G, Dahl JA, Niu Y, Fedorcsak P, Huang CM, Li CJ, et al. ALKBH5 is a mammalian RNA demethylase that impacts RNA metabolism and mouse fertility. *Mol Cell* 2013;**49**:18−29.
17. Shen D, Wang B, Gao Y, Zhao L, Bi Y, Zhang J, et al. Detailed resume of RNA m^6A demethylases. *Acta Pharm Sin B* 2022;**12**:2193−205.
18. Roundtree IA, Evans ME, Pan T, He C. Dynamic RNA modifications in gene expression regulation. *Cell* 2017;**169**:1187−200.
19. Huang H, Weng H, Chen J. m^6A modification in coding and non-coding RNAs: roles and therapeutic implications in cancer. *Cancer Cell* 2020;**37**:270−88.
20. Li ZH, Peng YX, Li JX, Chen ZJ, Chen F, Tu J, et al. *N*-6-Methyladenosine regulates glycolysis of cancer cells through PDK4. *Nat Commun* 2020;**11**:2578.
21. Chen ZJ, Wu L, Zhou JW, Lin X, Peng YX, Ge LC, et al. N^6-Methyladenosine-induced ERRγ triggers chemoresistance of cancer cells through upregulation of ABCB1 and metabolic reprogramming. *Theranostics* 2020;**10**:3382−96.
22. Wang Y, Li Y, Yue M, Wang J, Kumar S, Wechsler Reya RJ, et al. N^6-Methyladenosine RNA modification regulates embryonic neural stem cell self-renewal through histone modifications. *Nat Neurosci* 2018;**21**:195−206.
23. Barbieri I, Tzelepis K, Pandolfini L, Shi J, Millan Zambrano G, Robson SC, et al. Promoter-bound METTL3 maintains myeloid leukaemia by m^6A-dependent translation control. *Nature* 2017;**552**:126−31.
24. Slobodin B, Han R, Calderone V, Vrielink J, Loayza Puch F, Elkon R, et al. Transcription impacts the efficiency of mRNA translation *via* co-transcriptional N^6-adenosine methylation. *Cell* 2017;**169**:326−37. e12.
25. Liu J, Dou X, Chen C, Chen C, Liu C, Xu MM, et al. N^6-Methyladenosine of chromosome-associated regulatory RNA regulates chromatin state and transcription. *Science* 2020;**367**:580−6.
26. Li Y, Xia L, Tan K, Ye X, Zuo Z, Li M, et al. N^6-Methyladenosine co-transcriptionally directs the demethylation of histone H3K9me2. *Nat Genet* 2020;**52**:870−7.

27. Wu C, Chen W, He J, Jin S, Liu Y, Yi Y, et al. Interplay of m^{6}A and H3K27 trimethylation restrains inflammation during bacterial infection. *Sci Adv* 2020;**6**:eaba0647.
28. Jin X, Yan Y, Wang D, Ding D, Ma T, Ye Z, et al. DUB3 promotes BET inhibitor resistance and cancer progression by deubiquitinating BRD4. *Mol Cell* 2018;**71**:592−605.e4.
29. Lu L, Chen Z, Lin X, Tian L, Su Q, An P, et al. Inhibition of BRD4 suppresses the malignancy of breast cancer cells *via* regulation of Snail. *Cell Death Differ* 2020;**27**:255−68.
30. Tojkander S, Ciuba K, Lappalainen P. CaMKK2 regulates mechanosensitive assembly of contractile actin stress fibers. *Cell Rep* 2018;**24**:11−9.
31. Chang G, Shi L, Ye Y, Shi H, Zeng L, Tiwary S, et al. YTHDF3 induces the translation of m^{6}A-enriched gene transcripts to promote breast cancer brain metastasis. *Cancer Cell* 2020;**38**:857−71.e7.
32. Xiong J, He J, Zhu J, Pan J, Liao W, Ye H, et al. Lactylation-driven METTL3-mediated RNA m^{6}A modification promotes immunosuppression of tumor-infiltrating myeloid cells. *Mol Cell* 2022;**82**:1660−77. e10.
33. Huang H, Weng H, Sun W, Qin X, Shi H, Wu H, et al. Recognition of RNA N^6-methyladenosine by IGF2BP proteins enhances mRNA stability and translation. *Nat Cell Biol* 2018;**20**:285−95.
34. Chen F, Chen Z, Guan T, Zhou Y, Ge L, Zhang H, et al. N^6-Methyladenosine regulates mRNA stability and translation efficiency of KRT7 to promote breast cancer lung metastasis. *Cancer Res* 2021;**81**:2847−60.
35. Zepecki JP, Karambizi D, Fajardo JE, Snyder KM, Guetta Terrier C, Tang OY, et al. miRNA-mediated loss of m6A increases nascent translation in glioblastoma. *PLoS Genet* 2021;**17**:e1009086.
36. Zengerle M, Chan KH, Ciulli A. Selective small molecule induced degradation of the BET bromodomain protein BRD4. *Acs Chem Biol* 2015;**10**:1770−7.
37. Sobell HM. Actinomycin and DNA transcription. *Proc Natl Acad Sci U S A* 1985;**82**:5328−31.
38. Ge MK, Zhang N, Xia L, Zhang C, Dong SS, Li ZM, et al. FBXO22 degrades nuclear PTEN to promote tumorigenesis. *Nat Commun* 2020;**11**:1720.
39. Devaiah BN, Singer DS. Two faces of BRD4: mitotic bookmark and transcriptional lynchpin. *Transcription* 2013;**4**:13−7.
40. Zhou Q, Huang J, Zhang C, Zhao F, Kim W, Tu X, et al. The bromodomain containing protein BRD-9 orchestrates RAD51−RAD54 complex formation and regulates homologous recombination-mediated repair. *Nat Commun* 2020;**11**:2639.
41. Fujisawa T, Filippakopoulos P. Functions of bromodomain-containing proteins and their roles in homeostasis and cancer. *Nat Rev Mol Cell Bio* 2017;**18**:246−62.
42. Yu S, Kim VN. A tale of non-canonical tails: gene regulation by post-transcriptional RNA tailing. *Nat Rev Mol Cell Bio* 2020;**21**:542−56.
43. Paz I, Kosti I, Ares Jr M, Cline M, Mandel Gutfreund Y. RBPmap: a web server for mapping binding sites of RNA-binding proteins. *Nucleic Acids Res* 2014;**42**:W361−7.
44. Cornen S, Guille A, Adelaide J, Addou Klouche L, Finetti P, Saade MR, et al. Candidate luminal B breast cancer genes identified by genome, gene expression and DNA methylation profiling. *PLoS One* 2014;**9**:e81843.
45. Zhang N, Ge G, Meyer R, Sethi S, Basu D, Pradhan S, et al. Overexpression of separase induces aneuploidy and mammary tumorigenesis. *Proc Natl Acad Sci U S A* 2008;**105**:13033−8.
46. Hellmuth S, Gomez HL, Pendas AM, Stemmann O. Securin-independent regulation of separase by checkpoint-induced shugoshin-MAD2. *Nature* 2020;**580**:536−41.
47. Szasz AM, Lanczky A, Nagy A, Forster S, Hark K, Green JE, et al. Cross-validation of survival associated biomarkers in gastric cancer using transcriptomic data of 1065 patients. *Oncotarget* 2016;**7**:49322−33.
48. Wu SY, Nin DS, Lee AY, Simanski S, Kodadek T, Chiang CM. BRD4 phosphorylation regulates HPV E2-mediated viral transcription, origin replication, and cellular MMP-9 expression. *Cell Rep* 2016;**16**:1733−48.
49. Wu SY, Lee AY, Lai HT, Zhang H, Chiang CM. Phospho switch triggers Brd4 chromatin binding and activator recruitment for gene-specific targeting. *Mol Cell* 2013;**49**:843−57.
50. Stathis A, Bertoni F. BET proteins as targets for anticancer treatment. *Cancer Discov* 2018;**8**:24−36.
51. Donati B, Lorenzini E, Ciarrocchi A. BRD4 and cancer: going beyond transcriptional regulation. *Mol Cancer* 2018;**17**:164.
52. Sun C, Yin J, Fang Y, Chen J, Jeong KJ, Chen X, et al. BRD4 inhibition is synthetic lethal with PARP inhibitors through the induction of homologous recombination deficiency. *Cancer Cell* 2018;**33**:401−16. e8.
53. Floyd SR, Pacold ME, Huang Q, Clarke SM, Lam FC, Cannell IG, et al. The bromodomain protein Brd4 insulates chromatin from DNA damage signalling. *Nature* 2013;**498**:246−50.
54. Li X, Baek G, Ramanand SG, Sharp A, Gao Y, Yuan W, et al. BRD4 promotes DNA repair and mediates the formation of TMPRSS2-ERG gene rearrangements in prostate cancer. *Cell Rep* 2018;**22**:796−808.
55. Akincilar SC, Khattar E, Boon PL, Unal B, Fullwood MJ, Tergaonkar V. Long-range chromatin interactions drive mutant TERT promoter activation. *Cancer Discov* 2016;**6**:1276−91.
56. Brown JD, Lin CY, Duan Q, Griffin G, Federation A, Paranal RM, et al. NF-κB directs dynamic super enhancer formation in inflammation and atherogenesis. *Mol Cell* 2014;**56**:219−31.
57. Zhou KI, Shi H, Lyu R, Wylder AC, Matuszek Z, Pan JN, et al. Regulation of co-transcriptional pre-mRNA splicing by m^{6}A through the low-complexity protein hnRNPG. *Mol Cell* 2019;**76**:70−81.e9.
58. Wang X, Wang J, Tsui YM, Shi C, Wang Y, Zhang X, et al. RALYL increases hepatocellular carcinoma stemness by sustaining the mRNA stability of TGF-β2. *Nat Commun* 2021;**12**:1518.
59. Chiang CM. Phospho-BRD4: transcription plasticity and drug targeting. *Drug Discov Today Technol* 2016;**19**:17−22.
60. Matzuk MM, McKeown MR, Filippakopoulos P, Li Q, Ma L, Agno JE, et al. Small-molecule inhibition of BRDT for male contraception. *Cell* 2012;**150**:673−84.
61. Papi M, Berdougo E, Randall CL, Ganguly S, Jallepalli PV. Multiple roles for separase auto-cleavage during the G2/M transition. *Nat Cell Biol* 2005;**7**:1029−35.
62. Zhang NG, Pati D. Biology and insights into the role of cohesin protease separase in human malignancies. *Biol Rev* 2017;**92**:2070−83.
63. Mukherjee M, Ge G, Zhang N, Edwards DG, Sumazin P, Sharan S, et al. MMTV-*Espl1* transgenic mice develop aneuploid, estrogen receptor alpha (ERα)-positive mammary adenocarcinomas. *Oncogene* 2014;**33**:5511−22.
64. Shen C, Sheng Y, Zhu AC, Robinson S, Jiang X, Dong L, et al. RNA demethylase ALKBH5 selectively promotes tumorigenesis and cancer stem cell self-renewal in acute myeloid leukemia. *Cell Stem Cell* 2020;**27**:64−80.e9.
65. Zhang S, Zhao BS, Zhou A, Lin K, Zheng S, Lu Z, et al. m^{6}A demethylase ALKBH5 maintains tumorigenicity of glioblastoma stem-like cells by sustaining FOXM1 expression and cell proliferation program. *Cancer Cell* 2017;**31**:591−606.e6.
66. Choe J, Lin S, Zhang W, Liu Q, Wang L, Ramirez Moya J, et al. mRNA circularization by METTL3−eIF3h enhances translation and promotes oncogenesis. *Nature* 2018;**561**:556−60.